IMMUNOLOGY

Glycogen synthase kinase 3 drives thymocyte egress by suppressing β-catenin activation of Akt

Chenfeng Liu[1†], Lei Ma[1†], Yuxuan Wang[1†], Jiayi Zhao[1], Pengda Chen[1], Xian Chen[1], Yingxin Wang[1], Yanyan Hu[1], Yun Liu[1], Xian Jia[1], Zhanghua Yang[1], Xingzhi Yin[1], Jianfeng Wu[1], Suqin Wu[1], Haiping Zheng[1], Xiaohong Ma[1], Xiufeng Sun[1], Ying He[1], Lianghua Lin[1], Yubing Fu[1], Kunyu Liao[1], Xiaojuan Zhou[1], Shan Jiang[1], Guofeng Fu[1], Jian Tang[1], Wei Han[1], Xiao Lei Chen[1‡], Wenzhu Fan[1], Yazhen Hong[1], Jiahuai Han[1], Xiangyang Huang[2], Bo-An Li[1], Nengming Xiao[1], Changchun Xiao[1,3]*, Guo Fu[1]*[‡], Wen-Hsien Liu[1]*[§]

Molecular pathways controlling emigration of mature thymocytes from thymus to the periphery remain incompletely understood. Here, we show that T cell–specific ablation of glycogen synthase kinase 3 (GSK3) led to severely impaired thymic egress. In the absence of GSK3, β-catenin accumulated in the cytoplasm, where it associated with and activated Akt, leading to phosphorylation and degradation of Foxo1 and downregulation of Klf2 and $S1P_1$ expression, thereby preventing emigration of thymocytes. A cytoplasmic membrane-localized β-catenin excluded from the nucleus promoted Akt activation, suggesting a new function of β-catenin independent of its role as a transcriptional activator. Furthermore, genetic ablation of β-catenin, retroviral expression of a dominant negative Akt mutant, and transgenic expression of a constitutively active Foxo1 restored emigration of GSK3-deficient thymocytes. Our findings establish an essential role for GSK3 in thymocyte egress and reveal a previously unidentified signaling function of β-catenin in the cytoplasm.

INTRODUCTION

T cells develop in the thymus where they interact with a large array of highly spatially organized stromal cells that deliver signals essential for thymocyte survival, migration, proliferation, differentiation, and T cell receptor (TCR) repertoire selection. In the cortex of thymus, preselection $CD4^+CD8^+$ double-positive (DP) immature thymocytes migrate slowly in an apparent random walk, scanning cortex thymic epithelial cells (cTECs) with their TCRs for self-peptide–major histocompatibility complex (MHC) complexes. It is thought that DP thymocytes engage self-peptide–MHC complexes displayed by multiple cTECs, progressively integrating these transient TCR signaling events to reach a threshold for positive selection. Within hours of initiating positive selection, DP thymocytes up-regulate CD69 and chemokine receptors CCR4 and CCR7, whose ligands are produced by dendritic cells and epithelial cells in the thymic medulla (mTECs). Chemotaxis mediated by these chemokine receptors drives the migration of post-selection DP thymocytes into the medulla, accompanied by down-regulation of one of the coreceptors (CD4 or CD8) and differentiation into $CD4^+CD8^-$ or $CD4^-CD8^+$ single-positive (SP) thymocytes. Dendritic cells and mTECs are the major antigen-presenting cells in the thymic medulla, where they ectopically express and present tissue-restricted antigens. Any given tissue-restricted antigen is presented by only a small fraction of dendritic cells and mTECs. Therefore, SP thymocytes must efficiently scan these medullary antigen-presenting cells for cognate antigens. This is achieved by rapid SP thymocyte motility driven by CCR7 and G protein–coupled receptor 183 (GPR183) in response to their ligands produced by mTECs. SP thymocytes whose TCRs engage self-peptide–MHC complexes with high affinity and thereby trigger strong signals undergo apoptosis (negative selection) or are directed to several small subpopulations that include natural $Foxp3^+$ regulatory T cells (nT_{reg}), invariant natural killer T cells (iNKT), the precursors to $CD8\alpha^+$ intraepithelial lymphocytes (nIELp), and natural interleukin-17 (IL-17)–producing T helper cells (nT_H17) through a process called agonist selection. Only SP thymocytes whose TCRs engage self-peptide–MHC complexes with low affinity successfully emigrate from the thymus to join the peripheral T cell pool (*1*–*4*) .

During their time within the medulla, SP thymocytes go through a program of post-selection maturation, which is associated with up-regulation of CD62L, Klf2, $S1P_1$, Qa2, and MHC class I molecules and down-regulation of CD24 and CD69 (*1*). Mature SP thymocytes emigrate from the thymus via blood vessels at the corticomedullary junction in response to a S1P gradient established by pericytes, endothelial cells, and medullary stromal cells. Expression of $S1P_1$, a G protein–coupled receptor for S1P, plays a central role in thymocyte egress (*5*–*9*). Previous studies suggested that $S1P_1$ expression is controlled by TCR signaling (*2*). In semimature $CD69^+$ SP thymocytes that are receiving or have recently received activating signals through TCR engagement of self-peptide–MHC complexes, Foxo1 is phosphorylated by Akt, leading to cytosolic translocation and degradation of Foxo1 by the ubiquitin-proteasome pathway. Down-regulation of nuclear Foxo1 protein levels causes reduced transcription of Klf2 and $S1P_1$, resulting in thymic retention, maturation, and negative selection of these SP thymocytes. In addition, TCR engagement of self-peptide–MHC complexes up-regulates CD69, which associates with $S1P_1$ and inhibits the function of this receptor by inducing its internalization and degradation. Fully matured SP thymocytes are CD69 negative, indicating the termination

[1]State Key Laboratory of Cellular Stress Biology, Innovation Center for Cell Signaling Network, School of Life Sciences, Xiamen University, Xiamen, Fujian 361102, China. [2]Department of Rheumatology and Immunology, The Second Xiangya Hospital, Central South University, Changsha, Hunan 410011, China. [3]Department of Immunology and Microbiology, The Scripps Research Institute, La Jolla, CA 92037, USA.
*Corresponding author. Email: whliu@xmu.edu.cn (W.-H.L.); guofu@xmu.edu.cn (G.F.); cxiao@xmu.edu.cn (C.X.)
†These authors contributed equally to this work.
‡Present address: State Key Laboratory of Cellular Stress Biology, School of Medicine, Xiamen University, Xiamen, China.
§Lead contact.

of TCR signaling. This results in accumulation of Foxo1 in the nucleus and increased expression of Klf2 and $S1P_1$, which are essential for thymic egress (*2*). However, it is not clear why TCR signaling would diminish and why egress would occur as SP thymocytes mature, given the abundance of self-peptide–MHC complexes in the medulla (*1*).

Here, we identified glycogen synthase kinase 3 (GSK3) as a critical driver of thymocyte egress. GSK3 was discovered in 1980 as one of several kinases that phosphorylate glycogen synthase, the enzyme that catalyzes the rate-limiting step in glycogen synthesis. In the following decades, it was found that engagement of insulin receptor by insulin activates the phosphatidylinositol 3-kinase (PI3K)–Akt pathway, leading to phosphorylation of GSK3 by Akt at a serine residue near the N terminus of GSK3. Phosphorylation by Akt suppresses the activity of GSK3, promoting dephosphorylation (through the action of protein phosphatases) and activation of glycogen synthase, thus contributing to insulin-induced stimulation of glycogen synthesis (*10*). Over the years, a large diversity of cellular functions has been attributed to GSK3, such as cell differentiation, proliferation, transformation, and survival. Extensive studies have identified more than 100 substrates for GSK3 and shown that GSK3 activity promotes distinct outcomes in different types of cells (*11*, *12*). Nevertheless, the cellular context-specific functions of GSK3 and the underlying molecular mechanisms remain to be unraveled.

GSK3 is a ubiquitously expressed kinase with two isoforms, α and β, which are highly homologous within their kinase domains, show similar substrate specificities, and display largely redundant functions (*11*, *12*). Previous studies found that GSK3 plays important roles in T cell development, activation, and differentiation into effector cells (*13*–*18*). These studies primarily used chemical inhibitors and small interfering RNAs (siRNAs) to inhibit GSK3 activity, retroviral vectors to express constitutively active GSK3, or genetic approaches to delete individual GSK3 genes (α or β). The potential off-target effects of chemical inhibitors and siRNAs, the cell nonautonomous actions of chemical inhibitors when administered systemically, and the functional redundancy of GSK3α and GSK3β call into question whether these studies have revealed the true physiological roles of GSK3. To directly investigate GSK3 function in T cells, we genetically ablated both GSK3α and GSK3β genes in a T cell–specific manner. We found that GSK3 plays a critical role in controlling thymocyte egress through destabilizing β-catenin. In the absence of GSK3, β-catenin accumulated in the cytoplasm, where it associated with and activated Akt by decreasing Akt interactions with phosphatases PHLPP2 and PP2A, resulting in phosphorylation and degradation of Foxo1, down-regulation of Klf2 and $S1P_1$ expression, and impaired thymocyte egress. Moreover, genetic ablation of β-catenin, retroviral expression of a dominant negative (DN) Akt mutant, and transgenic expression of a constitutively active Foxo1 restored emigration of GSK3-deficient thymocytes. Therefore, this study establishes an essential role for GSK3 in thymocyte egress and reveals a novel signaling function of β-catenin in the cytoplasm.

RESULTS

Impaired generation of peripheral T cells in *Gsk3a*$^{fl/fl}$*Gsk3b*$^{fl/fl}$*CD4*-Cre mice

We examined the expression of GSK3α and GSK3β in $CD4^-CD8^-$ (DN), $CD4^+CD8^+$ (DP), $CD4^+$ and $CD8^+$ SP thymocytes, as well as peripheral $CD4^+$ and $CD8^+$ T cells by immunoblot analysis. GSK3α and GSK3β were constitutively expressed in the T lineage cells (Fig. 1A). To reveal the physiological roles of GSK3 in T cell development, we crossed mice harboring *loxP*-flanked *Gsk3α* (*Gsk3a*$^{fl/fl}$) or *Gsk3β* (*Gsk3b*$^{fl/fl}$) alleles with *Cd4*-Cre mice, which express the Cre recombinase under the control of the T cell–specific *CD4* promoter (*19*, *20*). Deletion of GSK3 in *Gsk3a*$^{fl/fl}$*Gsk3b*$^{fl/fl}$*Cd4*-Cre (hereafter referred to as *Gsk3a*$^{-/-}$*b*$^{-/-}$ or DKO) mice was confirmed by immunoblot analysis of CD4 and CD8 SP thymocytes (Fig. 1B). *Gsk3a*$^{-/-}$*b*$^{-/-}$ mice showed marked reduction in the percentages and numbers of $CD4^+$ and $CD8^+$ T cells in the spleen and lymph nodes (Fig. 1, C to F). Most of the remaining peripheral $CD4^+$ and $CD8^+$ T cells exhibited the phenotypes of activated and effector T cells (Fig. 1, G and H). The percentages, numbers, and activation status of $CD4^+$ and $CD8^+$ T cells in the spleen and lymph nodes of *Gsk3a*$^{fl/fl}$*Cd4*-Cre (*Gsk3a*$^{-/-}$) and *Gsk3b*$^{fl/fl}$*Cd4*-Cre (*Gsk3b*$^{-/-}$) mice were largely normal (fig. S1), suggesting that GSK3 plays an essential role in T cell development and that its two isoforms (GSK3α and GSK3β) are functionally redundant in this process.

GSK3 controls survival and egress of SP thymocytes

We analyzed thymocyte development in *Gsk3a*$^{-/-}$*b*$^{-/-}$ mice. Consistent with Cre recombinase expression being turned on in DP thymocytes in the *Cd4*-Cre mice (*21*), *Gsk3a*$^{-/-}$*b*$^{-/-}$ mice exhibited largely normal development of DN thymocytes, with a slight reduction in the number of DP thymocytes and a substantial decrease in both the percentages and numbers of $CD4^+$ and $CD8^+$ SP thymocytes (fig. S2, A and B). To identify the developmental block in the *Gsk3a*$^{-/-}$*b*$^{-/-}$ mice, we divided thymocytes into five populations based on their expression of CD3 and CD69 and then analyzed the expression of CD4 and CD8 (*22*). Populations 1 to 4, which included DN to post-positive selection thymocytes, were present in similar percentages and numbers in the *Gsk3a*$^{-/-}$*b*$^{-/-}$ and wild-type (WT) mice. Population 5, which had a $TCR^{hi}CD69^{lo}$ phenotype and corresponded to mature SP thymocytes ready for emigration to the periphery, was mostly absent in *Gsk3a*$^{-/-}$*b*$^{-/-}$ mice, suggesting that thymocyte development was blocked at the maturation or egress stages of SP thymocytes (fig. S2, C to E). A recent study showed that GSK3 controlled cell size, proliferation, and survival of B cells (*23*). Similarly, GSK3-deficient SP thymocytes showed significant increases in cell size and proliferation (fig. S3, A to D). IL-7 signaling is required for maintaining T cell survival and preventing the mitochondrial pathway of apoptosis by inducing the expression of Bcl-2 (*24*). As shown in fig. S3 (E to H), Bcl-2 expression was decreased, whereas IL-7R expression was slightly increased in GSK3-deficient SP thymocytes. When cultured in vitro with IL-7, GSK3-deficient SP thymocytes were more susceptible to apoptosis, accompanied by reduced expression of Bcl-2 (fig. S3, I to N).

Increased apoptosis may contribute to the diminished numbers of SP thymocytes (fig. S2, A and B) but does not explain the nearly complete absence of T cells in the spleen and lymph nodes of *Gsk3a*$^{-/-}$*b*$^{-/-}$ mice. To investigate whether GSK3 regulates the egress of mature thymocytes to the periphery, *Gsk3a*$^{-/-}$*b*$^{-/-}$ and WT mice were injected with fluorescein isothiocyanate (FITC) intrathymically to label thymocytes. One day after FITC injection, 1 to 2% of T cells in the spleen and lymph nodes of WT mice were FITC-labeled, and they were recent thymic emigrants. In contrast, very few $FITC^+$ T cells were detected in the spleen of *Gsk3a*$^{-/-}$*b*$^{-/-}$ mice, accompanied by elevated accumulation of $FITC^+$ CD4 and CD8 SP thymocytes in the thymus (Fig. 2, A to D), suggesting impaired egress of SP thymocytes in these animals. We next investigate whether GSK3

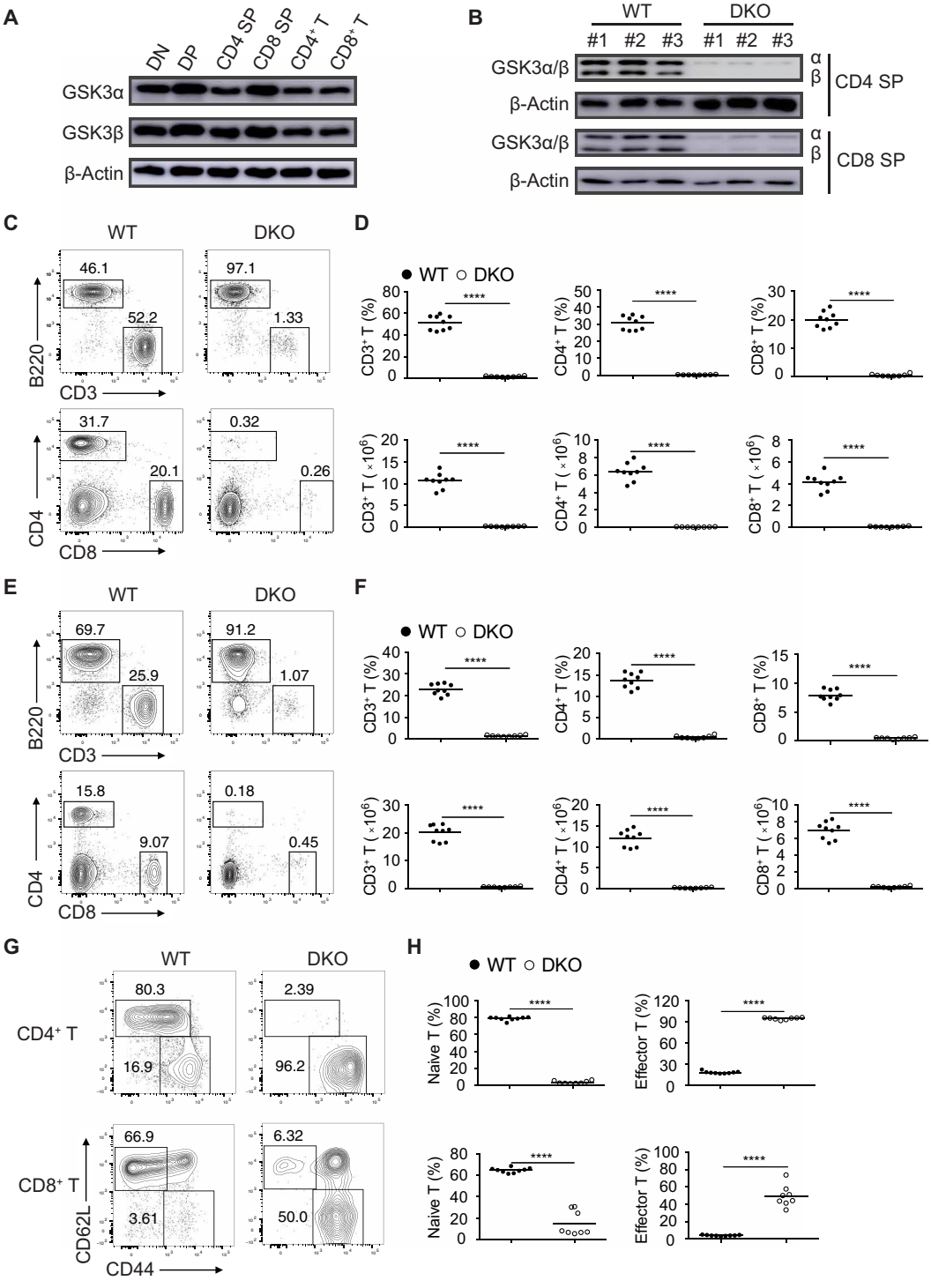

Fig. 1. T cell lymphopenia in mutant mice with T cell–specific deletion of GSK3. (**A**) Immunoblot analysis of GSK3α and GSK3β in DN, DP, CD4, and CD8 SP thymocytes and peripheral CD4$^+$ and CD8$^+$ T cells. (**B**) Immunoblot analysis of GSK3α and GSK3β in CD4 and CD8 SP thymocytes from wild-type (WT) and *Gsk3a*$^{-/-}$*b*$^{-/-}$ (DKO) mice. Numbers indicate three mice per group. (**C** to **F**) Flow cytometry analysis of CD3$^+$ T and B220$^+$ B cells (top) and CD4$^+$ and CD8$^+$ T cells (bottom) in the lymph nodes (C) and spleen (E) of 4- to 6-week-old WT and DKO mice. Summary of the percentage and number of CD3$^+$ T cells (left), CD4$^+$ T cells (middle), and CD8$^+$ T cells (right) in the lymph nodes (D) and spleen (F) of WT and DKO groups ($n \geq 8$ per group). (**G**) Flow cytometry analysis of naive (CD62L$^+$CD44$^-$) and activated (CD62L$^-$CD44$^+$) T cells among CD4$^+$ and CD8$^+$ T cells in the spleen of WT and DKO mice. (**H**) Summary of the percentages of naive and activated T cells from (G). Each symbol represents an individual mouse; small horizontal lines indicate the mean (± SEM). ****$P < 0.0001$. Data are representative of at least three independent experiments.

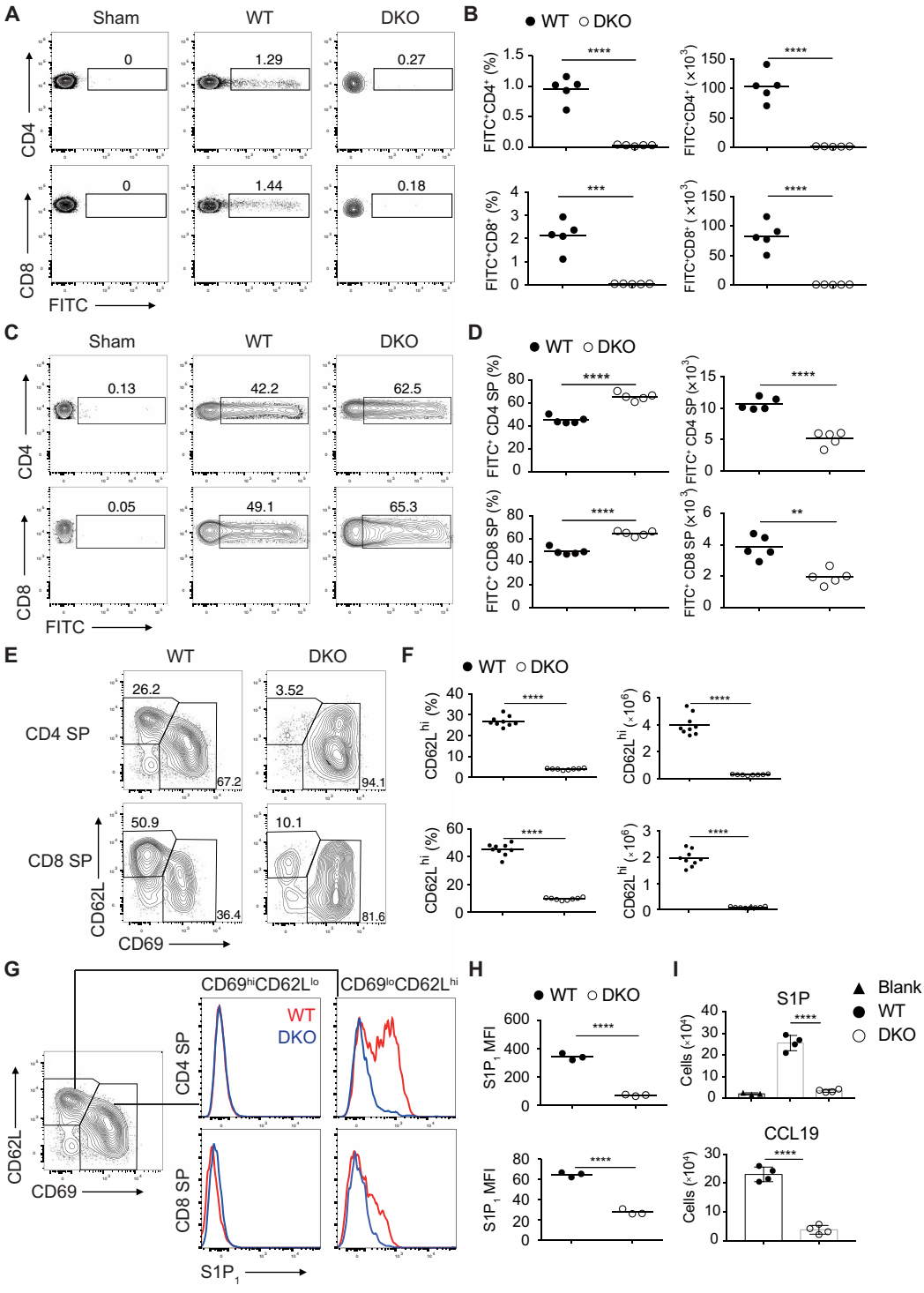

Fig. 2. GSK3 is essential for thymocyte egress and regulates $S1P_1$ expression on mature thymocytes. FITC-labeled cells in the spleen (**A**) and thymus (**C**) from WT and DKO mice 1 day after intrathymic FITC injection were analyzed by flow cytometry. (**B** and **D**) The percentage of FITC-labeled $CD4^+$ or $CD8^+$ T cells was calculated as described in Materials and Methods ($n = 5$ per group). (**E**) Flow cytometry analysis of CD62L and CD69 expression on CD4 and CD8 SP thymocytes from 4- to 6-week-old WT and DKO mice. (**F**) Percentage and numbers of $CD62L^{hi}CD69^{lo}$ cells among CD4 (top) or CD8 (bottom) SP thymocytes from (E). (**G** and **H**) $S1P_1$ expression on $CD62L^{hi}CD69^{lo}$ and $CD62L^{lo}CD69^{hi}$ cells from CD4 (top) and CD8 (bottom) SP thymocytes from 4- to 6-week-old WT and DKO mice. (G) Representative FACS plots. (H) Summary of mean fluorescence intensity (MFI) of $S1P_1$ in (G). (**I**) Transwell migration assay of DKO and WT CD4 SP thymocytes in response to S1P (top) and CCL19 (bottom). Each symbol represents an individual mouse. Small horizontal lines indicate the mean (± SEM). $^{**}P < 0.01$; $^{***}P < 0.001$; $^{****}P < 0.0001$. Data are representative of at least two (A, B, and I) and three (E to H) independent experiments.

deficiency also affects homing of SP thymocytes to the lymph nodes. Sorted CD4 SP thymocytes from WT (Thy1.1$^+$) and *Gsk3a*$^{-/-}$ (Thy1.2$^+$) or *Gsk3a*$^{-/-}$*b*$^{-/-}$ (Thy1.2$^+$) mice were cotransferred to CD45.1$^+$ mice. One day after transfer, significant numbers of *Gsk3a*$^{-/-}$ CD4 SP T cells were detected in the blood, spleen, and lymph nodes of recipient mice, while very few *Gsk3a*$^{-/-}$*b*$^{-/-}$ CD4 SP T cells were found there (fig. S4). Together, these results support a critical role for GSK3 in regulating the survival, egress, and periphery homing of SP thymocytes.

GSK3 regulates expression of molecules controlling thymocyte egress

Down-regulation of CD69 and up-regulation of S1P$_1$ play pivotal roles in promoting the egress of mature thymocytes (*2*). Consistent with their impaired emigration from the thymus, GSK3-deficient SP thymocytes were severely compromised in S1P$_1$ up-regulation and CD69 down-regulation (Fig. 2, E to H). The expression of other surface molecules previously implicated in thymocyte maturation and migration was also examined. CD3, CD5, CD44, and CD62L exhibited similar expression patterns on GSK3-deficient and WT SP thymocytes (fig. S5, A to D). The expression of CCR7, which drives the migration of post-selection DP thymocytes from cortex into medulla, increases SP thymocyte motility in the medulla, and promotes the homing and retention of naive T cells in secondary lymphoid organs (*1*), was significantly decreased on GSK3-deficient SP thymocytes (fig. S5, C and D). In contrast, expression of CXCR4, which mediates SDF1-driven repulsion of SP thymocytes away from the thymus (*25*, *26*), was much higher on GSK3-deficient SP thymocytes, likely due to compensatory mechanisms in response to defective S1P$_1$ and CCR7 expression on these cells (fig. S5, C and D). To determine whether GSK3 regulates S1P$_1$- and CCR7-mediated cell migration of SP thymocytes, we performed in vitro migration assay in transwells. *Gsk3a*$^{-/-}$*b*$^{-/-}$ CD4 SP thymocytes exhibited impaired S1P- and CCL19-induced cell migration (Fig. 2I).

Positively selected medullary thymocytes (CCR7$^+$TCRβ$^+$) can be further divided into semimature M1 and M2 subpopulations based on the expression of CD69 and MHC class I (MHCI) (*27*). The frequency of CCR7$^+$TCRβ$^+$ cells was decreased in *Gsk3a*$^{-/-}$*b*$^{-/-}$ thymocytes, accompanied by increased percentages of M1 (CD69$^+$MHCI$^+$) but decreased percentages of M2 cells (CD69$^-$MHCI$^+$). The percentages of CD4 and CD8 SP thymocytes among M1 and M2 cells were similar in *Gsk3a*$^{-/-}$*b*$^{-/-}$ and WT mice (fig. S5, E to G). Only a fraction of M2 cells expressed high levels of CD62L and S1P$_1$, representing mature SP thymocytes competent for emigration (*27*). These S1P$_1^{hi}$CD62L^{hi} cells were nearly absent in *Gsk3a*$^{-/-}$*b*$^{-/-}$ mice (fig. S5, H to J), which is consistent with severely compromised thymocyte egress in these animals. Notably, significantly higher percentage of SP thymocytes in *Gsk3a*$^{-/-}$*b*$^{-/-}$ mice expressed the maturation marker Qa2, suggesting accumulation of mature thymocytes caused by impaired egress (fig. S5, A and B). GSK3-deficient CD8 SP thymocytes failed to down-regulate CD24 or to up-regulate β7-integrin, the latter of which is required for T cell migration to the gut (fig. S5, A to D) (*28*). The expression of these two molecules was normal on GSK3-deficient CD4 SP thymocytes, in line with previous studies showing that the medullary stage of thymocyte development and maturation differs between CD4 and CD8 SP thymocytes (*29*, *30*). Therefore, GSK3 regulates the expression of molecules that control thymocyte egress.

As the expression of Cre recombinase is turned on in preselection DP thymocytes in the *Cd4*-Cre mice (*20*, *21*), it is possible that deletion of the *GSK3* genes affects the selection of DP thymocytes, resulting in altered TCR repertoire, which leads to impaired survival and egress of mature thymocytes. To address this issue, we introduced two TCR transgenes into *Gsk3a*$^{-/-}$*b*$^{-/-}$ mice: OT-II and P14. CD4$^+$ T cells express transgenic chick ovalbumin$_{323–339}$-specific αβ-TCR in the context of I-A^b in OT-II mice (*31*), while CD8$^+$ T cells expressed TCR specific for lymphocytic choriomeningitis virus (LCMV) GP$_{33–41}$ presented by H-2D^b in P14 mice (*32*). DP thymocytes expressing these two TCRs undergo positive selection and develop into CD4 and CD8 SP thymocytes, respectively. Similar to *Gsk3a*$^{-/-}$*b*$^{-/-}$ mice, both *Gsk3a*$^{-/-}$*b*$^{-/-}$OT-II and *Gsk3a*$^{-/-}$*b*$^{-/-}$P14 mice exhibited much reduced T cell numbers in the spleen and lymph nodes, as well as impaired S1P$_1$ up-regulation and CD69 down-regulation on SP thymocytes (figs. S6 and S7). In addition, *Gsk3a*$^{-/-}$*b*$^{-/-}$OT-II mice showed a reduction in the numbers of DP and CD4 SP thymocytes (fig. S6F), which is comparable to *Gsk3a*$^{-/-}$*b*$^{-/-}$ mice (fig. S2B). There is no decrease in the number of DP thymocytes and a slight increase in the number of CD8 SP thymocytes in *Gsk3a*$^{-/-}$*b*$^{-/-}$P14 mice (fig. S7F). Together, these data suggest that GSK3 deficiency may affect thymocyte selection and cause the death of some T cell clones, which would have survived in WT mice, resulting in a reduction in the numbers of DP and CD4 SP thymocytes in *Gsk3a*$^{-/-}$*b*$^{-/-}$ mice. Nevertheless, thymocyte egress was similarly impaired in all these three strains of mice, indicating that it is quite unlikely that impaired thymus egress in *Gsk3a*$^{-/-}$*b*$^{-/-}$ mice is caused by altered TCR repertoire.

We next investigated whether GSK3 controls the survival and egress of thymocytes in a cell-intrinsic manner. Mixed bone chimeras were generated by reconstituting irradiated *Rag2*$^{-/-}$ mice with bone marrow cells from *Gsk3a*$^{-/-}$*b*$^{-/-}$ (CD45.2$^+$) and WT CD45.1$^+$ and CD45.1$^+$ CD45.2$^+$ congenic donors (fig. S8A). Both the percentage and numbers of peripheral CD4$^+$ and CD8$^+$ T cells, but not B cells, derived from *Gsk3a*$^{-/-}$*b*$^{-/-}$ bone marrow cells were markedly reduced in the chimeras (fig. S8, B and C). There was a slight increase in the frequency of DP thymocytes but a decrease in the frequency of CD4 and CD8 SP thymocytes derived from *Gsk3a*$^{-/-}$*b*$^{-/-}$ bone marrow cells (fig. S8, D and E). Similar to *Gsk3a*$^{-/-}$*b*$^{-/-}$, *Gsk3a*$^{-/-}$*b*$^{-/-}$OT-II, and *Gsk3a*$^{-/-}$*b*$^{-/-}$P14 mice, GSK3-deficient SP thymocytes in the chimeras failed to down-regulate CD69 or to up-regulate S1P$_1$ and CCR7 (fig. S8, F to I). These results demonstrated that GSK3 controls thymocyte egress in a cell-intrinsic manner, while both cell-intrinsic and cell-extrinsic factors contribute to GSK3 regulation of thymocyte survival.

GSK3 regulates the Akt-Foxo1-Klf2 pathway in SP thymocytes

To gain insights into the molecular mechanisms underlying GSK3 regulation of thymocyte egress and survival, we performed transcriptome analysis of DP, CD4, and CD8 SP thymocytes from *Gsk3a*$^{-/-}$*b*$^{-/-}$ and WT mice. Principal components analysis (PCA) showed that the gene expression profiles of these cells were markedly affected by GSK3 deficiency (Fig. 3A). To better understand the detailed regulatory network controlled by GSK3, we analyzed signaling pathways and molecular functions enriched among differentially expressed genes and found that GSK3 controls genes involved in transcriptional regulation, lymphocyte egress, cell cycle, phosphatases, and kinases (Fig. 3, B and C). The genes down-regulated in *Gsk3a*$^{-/-}$*b*$^{-/-}$ SP thymocytes encoded several receptors involved in thymocyte egress and homing (Fig. 3C). Pathway analysis suggested

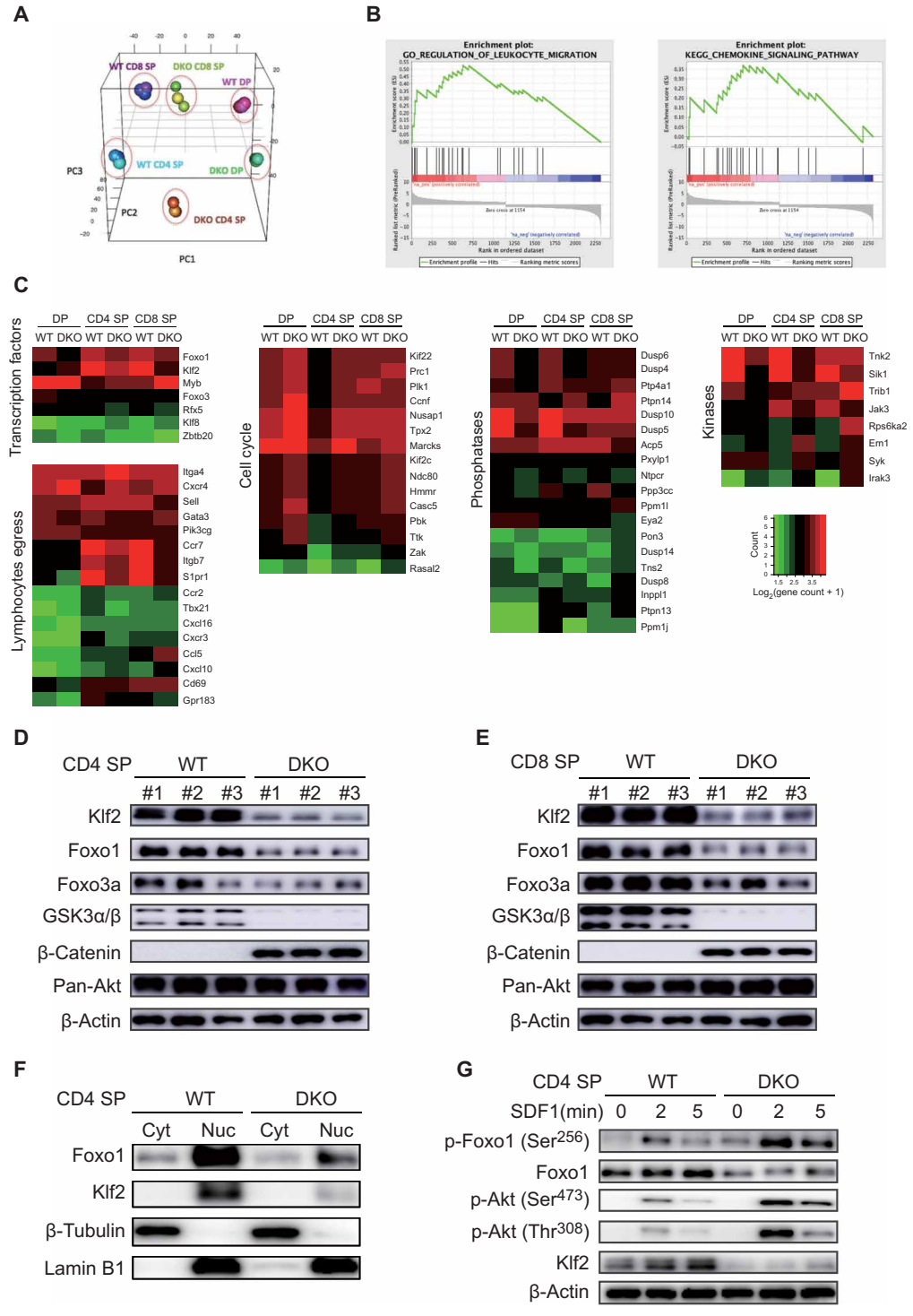

Fig. 3. GSK3 regulates the Akt-Foxo1-Klf2 pathway in SP thymocytes. (**A**) Principal components analysis (PCA) of RNA-seq data showed the distribution of DN, DP, CD4, and CD8 SP thymocytes from 6-week-old WT and DKO mice. (**B**) Gene set enrichment analysis (GSEA) using Hallmark gene sets showed that the leukocyte migration and chemokine signaling pathways were among the highest ranked gene signatures differentially enriched in WT and DKO DP, CD4 SP, and CD8 SP. (**C**) Differentially expressed genes between WT and DKO SP thymocytes were grouped by function. (**D** and **E**) Immunoblot analysis of the Akt-Foxo1-Klf2 pathway in CD4 (D) and CD8 (E) SP thymocytes from WT and DKO mice ($n = 3$ per group). (**F**) Immunoblot analysis of Foxo1, Klf2, β-tubulin, and lamin B1 in the cytoplasmic (Cyt) and nuclear (Nuc) fractions of CD4 SP thymocytes from WT and DKO mice. (**G**) Immunoblot analysis of the Akt-Foxo1-Klf2 pathway in CD4 SP thymocytes from WT and DKO mice stimulated with SDF1 for indicated amounts of time. Note the significant up-regulation of Akt phosphorylation of Foxo1 and marked reduction in Foxo1 and Klf2 protein expression in DKO CD4 SP thymocytes in the absence of SDF1 stimulation. Data are representative of at least three independent experiments.

that Foxo1-Klf2 signaling could be regulated by GSK3. Klf2, a target gene of Foxo1, plays a central role in controlling thymocyte egress and recirculation (*33*, *34*). Immunoblot analysis of CD4 and CD8 SP thymocytes showed that Klf2 expression was markedly reduced in GSK3-deficient SP thymocytes, accompanied by decreased expression of Foxo1 and β-catenin accumulation (Fig. 3, D and E). Nuclear accumulation of Klf2 and Foxo1 was also significantly decreased in GSK3-deficient CD4 SP thymocytes (Fig. 3F). Phosphorylation of Foxo1 by Akt leads to nucleus-to-cytosol translocation of Foxo1 and subsequent degradation of Foxo1 in the cytosol by the ubiquitin-proteasome pathway (*35*). To investigate whether GSK3 affects chemokine receptor signaling–induced Akt activation and Foxo1 phosphorylation, WT and $Gsk3a^{-/-}b^{-/-}$ CD4 SP thymocytes were stimulated with SDF1, followed by immunoblot analysis of downstream signaling pathways. As shown in Fig. 3G, SDF1-mediated phosphorylation of Akt and Foxo1 was all significantly increased in $Gsk3a^{-/-}b^{-/-}$ CD4 SP thymocytes, accompanied by reduced Foxo1 and Klf2 protein levels. It is worth noting that even before SDF1 simulation, $Gsk3a^{-/-}b^{-/-}$ CD4 SP thymocytes already exhibited obvious Akt phosphorylation of Foxo1 that was not seen in their WT counterparts, as well as much reduced protein levels of Foxo1 and Klf2. To examine the functional relevance of Foxo1 and Klf2 down-regulation to impaired egress of $Gsk3a^{-/-}b^{-/-}$ thymocytes, $Gsk3a^{-/-}b^{-/-}$ and WT CD4 SP thymocytes were transduced with retroviruses encoding Klf2 or Foxo1AAA, and their proliferation, survival, and migration were subsequently analyzed. The results showed that retroviral expression of Klf2 decreased proliferation and apoptosis of WT CD4 SP thymocytes, and rescued survival, but not proliferation, of $Gsk3a^{-/-}b^{-/-}$ CD4 SP thymocytes (fig. S9, A to C). In addition, Klf2 expression partially restored CD62L up-regulation and CD69 down-regulation (fig. S9D), and S1P- and CCL19-induced migration of $Gsk3a^{-/-}b^{-/-}$ CD4 SP thymocytes (fig. S9E). As shown in fig. S9 (F to H), Foxo1AAA expression did not affect the survival and proliferation of WT CD4 SP thymocytes. However, it largely restored the survival and S1P- and CCL19-induced migration, and partially restored the proliferation of $Gsk3a^{-/-}b^{-/-}$ CD4 SP thymocytes (fig. S9, F to I), suggesting that Foxo1 also controls the survival of CD4 SP thymocytes, in addition to its role in regulating thymocyte emigration. Together, these results suggested that GSK3 may control thymocyte egress through attenuation of the Akt-Foxo1-Klf2 signaling pathway and that GSK3 suppresses tonic Akt signaling in the absence of extracellular stimulation (*36*, *37*).

Constitutively active Foxo1 restores emigration of GSK3-deficient thymocytes

Previous studies found that Foxo1 controls the expression of CD62L, CCR7, and $S1P_1$ through Klf2 (*2*, *38*). To investigate the functional importance of Foxo1 in mediating GSK3 regulation of thymocyte egress, we crossed $Gsk3a^{-/-}b^{-/-}$ mice with $Foxo1^{AAA}$ mice that carry a conditional transgene of Foxo1 with three alanine amino acid substitutions at the Akt phosphorylation sites, rendering the mutant Foxo1 resistant to Akt phosphorylation, nucleus-to-cytosol translocation, and degradation (*39*). Foxo1AAA expression in CD4 SP thymocytes of the resulting mice was confirmed by flow cytometry and immunoblot analysis (Fig. 4, A and B). The percentage and number of peripheral $CD3^+TCR\beta^+$ T cells were substantially restored in $Gsk3a^{-/-}b^{-/-}Foxo1^{AAA}$ mice compared to $Gsk3a^{-/-}b^{-/-}$ and WT mice (Fig. 4, C and D). Further analysis showed that $CD8^+$ T cells were largely restored in $Gsk3a^{-/-}b^{-/-}Foxo1^{AAA}$ mice, whereas the percentage and number of $CD4^+$ T cells were much reduced in the periphery of $Foxo1^{AAA}$, $Gsk3a^{-/-}b^{-/-}$, and $Gsk3a^{-/-}b^{-/-}Foxo1^{AAA}$ mice (Fig. 4, E and F). This is consistent with a recent study showing that Akt phosphorylation of Foxo1 and its subsequent degradation are essential for CD4 T cell maintenance and that $Foxo1^{AAA}$*CD4-Cre* mice had much reduced numbers of CD4 T cells but normal numbers of CD8 T cells in the periphery (*40*). In addition, the thymi of $Foxo1^{AAA}$*CD4-Cre* mice were much smaller than their WT counterparts, probably due to the systemic autoimmunity caused by severely compromised maintenance of regulatory T cells (*40*). $Gsk3a^{-/-}b^{-/-}Foxo1^{AAA}$ mice exhibited no obvious symptoms of autoimmunity, and their thymi were normal in size and cellularity. This allowed a fair comparison of thymocyte egress in $Gsk3a^{-/-}b^{-/-}$ and $Gsk3a^{-/-}b^{-/-}Foxo1^{AAA}$ mice. There were slightly more CD4 SP thymocytes in $Gsk3a^{-/-}b^{-/-}Foxo1^{AAA}$ than in $Gsk3a^{-/-}b^{-/-}$ mice, while their numbers of CD8 SP thymocytes were comparable (Fig. 4, G and H). CD69 down-regulation and $S1P_1$ up-regulation on SP thymocytes were completely restored in $Gsk3a^{-/-}b^{-/-}Foxo1^{AAA}$ mice (Fig. 4, I to K). Protein levels of $S1P_1$, Klf2, and Foxo1 were also restored to WT levels in $Gsk3a^{-/-}b^{-/-}Foxo1^{AAA}$ CD4 SP thymocytes (Fig. 4L).

To determine whether Foxo1AAA restores the emigration of GSK3-deficient SP thymocytes out of the thymus and the homing of GSK3-deficient T cells to lymph nodes in a T cell–intrinsic manner, mature $CD4^+TCR\beta^+$ SP thymocytes from WT, $Gsk3a^{-/-}b^{-/-}$, and $Gsk3a^{-/-}b^{-/-}Foxo1^{AAA}$ mice were adoptively transferred into $CD45.1^+$ congenic recipients, followed by analysis of their appearance in the spleen and lymph nodes 24 hours later. When transferred through intrathymic injection, the emigration of $Gsk3a^{-/-}b^{-/-}Foxo1^{AAA}$ SP thymocytes out of the thymus was largely restored (fig. S10, A to C). When transferred intravenously, $Gsk3a^{-/-}b^{-/-}Foxo1^{AAA}$ SP thymocytes were also able to home to lymph nodes as efficiently as their WT counterparts (fig. S10, D to F). Together, these results demonstrate that Foxo1 plays a major role in mediating GSK3 regulation of thymocyte emigration out of the thymus and homing to lymph nodes in a T cell–intrinsic manner.

Elevated Akt activity impairs egress of GSK3-deficient thymocytes

GSK3-deficient SP thymocytes exhibited increased phosphorylation of Akt and Foxo1 and reduced Foxo1 protein levels (Fig. 3), suggesting that elevated Akt activity causes defective thymocyte egress. To test this possibility, bone marrow cells from WT and $Gsk3a^{-/-}b^{-/-}$ mice were transduced with retroviruses encoding an Akt DN mutant and used to reconstitute $Rag2^{-/-}$ mice, followed by analysis of T cell development in the recipients (*41*). We first confirmed Akt DN expression and its inhibitory effects on Akt activity in CD4 SP thymocytes from the recipients. As shown in fig. S11A, SDF1-induced Akt and Foxo1 phosphorylation was significantly reduced in Akt-DN–expressing WT CD4 SP thymocytes. The frequency and number of peripheral GSK3-deficient $CD4^+$ T cells were largely restored by Akt DN expression, while there was only a slight rescue of peripheral GSK3-deficient $CD8^+$ T cells (Fig. 5, A and B). Akt-DN expression did not change the development of GSK3-deficient thymocytes (Fig. 5, C and D) but substantially restored CD69 down-regulation and $S1P_1$ up-regulation on GSK3-deficient SP thymocytes, promoting their emigration from the thymus and homing to secondary lymph organs (Fig. 5, E to G). In addition, Akt-DN substantially restored the survival and CCL19- and S1P-stimulated migration (fig. S11B) and partially restored the proliferation

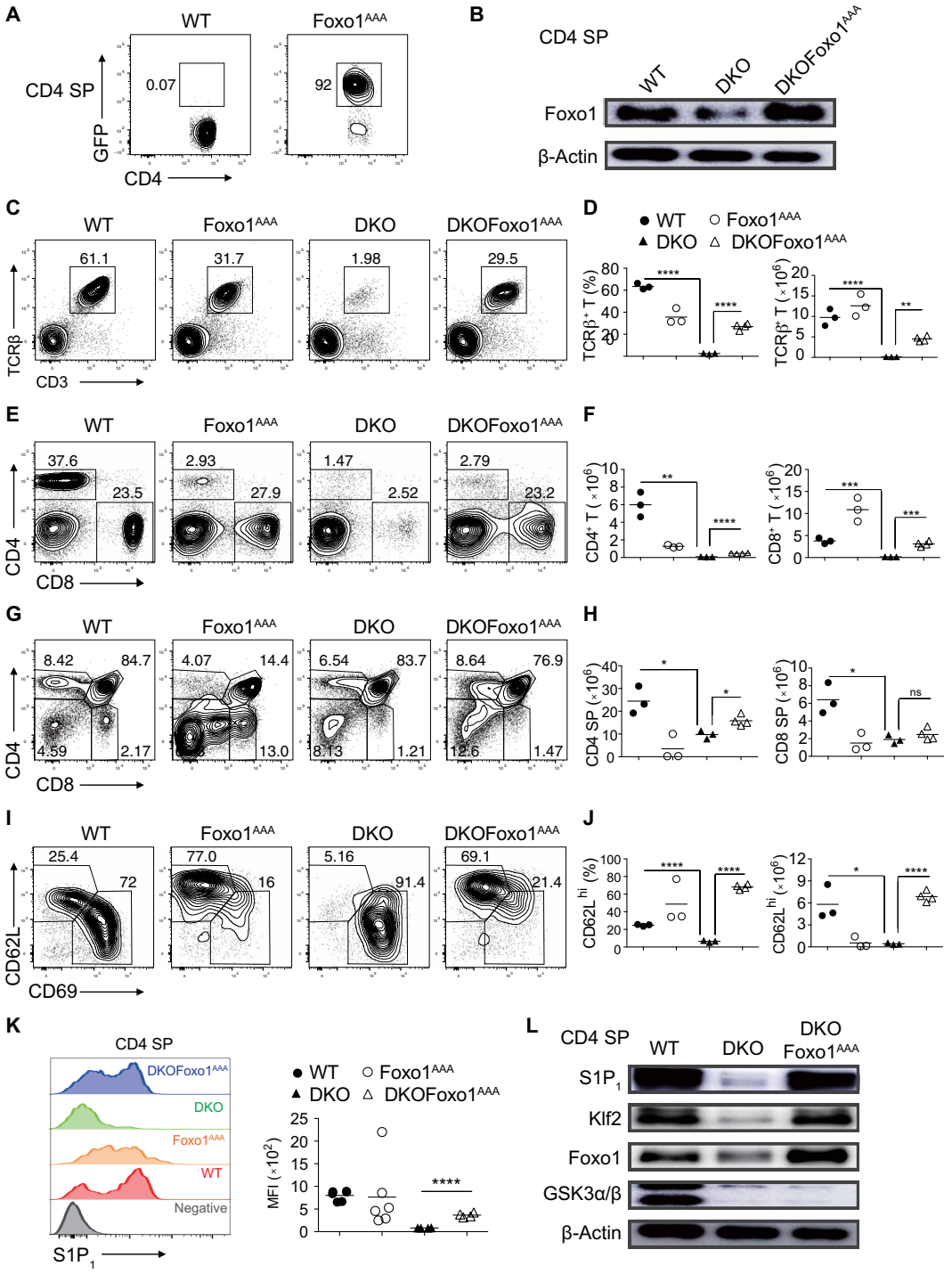

Fig. 4. Constitutively active Foxo1 restores the egress of GSK3-deficient thymocytes. (**A** and **B**) Flow cytometry and immunoblot analysis of the expression of a conditional transgene encoding constitutively active Foxo1 (Foxo1^{AAA}) and GFP in CD4 SP thymocytes from WT, Foxo1^{AAA}, DKO, and DKOFoxo1^{AAA} mice. (**C**) Flow cytometry analysis of CD3$^+$TCRβ$^+$ T cells in the lymph nodes of WT, Foxo1^{AAA}, DKO, and DKOFoxo1^{AAA} mice. (**D**) Summary of the percentage and number of CD3$^+$TCRβ$^+$ T cells in (C) ($n \geq 3$ per group). (**E**) Flow cytometry analysis of CD4$^+$ and CD8$^+$ T cells in the lymph nodes of WT, Foxo1^{AAA}, DKO, and DKOFoxo1^{AAA} mice. (**F**) Summary of the numbers of CD4$^+$ and CD8$^+$ T cells in (E) ($n \geq 3$ per group). (**G**) Flow cytometry analysis of thymocyte development in WT, Foxo1^{AAA}, DKO, and DKOFoxo1^{AAA} mice. (**H**) Summary of the numbers of CD4 and CD8 SP thymocytes in (G) ($n \geq 3$ per group). (**I**) Flow cytometry analysis of CD62L^{hi}CD69^{lo} and CD62L^{lo}CD69^{hi} cells among CD4 SP thymocytes from WT, Foxo1 AAA, DKO, and DKOFoxo1^{AAA} mice. (**J**) Summary of the percentage and number of CD62L^{hi}CD69^{lo} cells among CD4 SP thymocytes in (I) ($n \geq 3$ per group). (**K**) S1P$_1$ expression on CD62L^{hi}CD69^{lo} CD4 SP thymocytes from WT, Foxo1^{AAA}, DKO, and DKOFoxo1^{AAA} mice was analyzed by flow cytometry. CD62L^{lo}CD69^{hi} cells as a negative control (gray). Right: MFI of S1P$_1$ expression on CD62L^{hi}CD69^{lo} CD4 SP thymocytes of indicated genotypes. (**L**) Immunoblot analysis of S1P$_1$, Klf2, Foxo1, GSK3α/β, and β-actin in CD4 SP thymocytes from WT, DKO, and DKOFoxo1^{AAA} mice. Each symbol represents an individual mouse. Small horizontal lines indicate the mean (± SEM). *$P < 0.1$; **$P < 0.01$; ***$P < 0.001$; ****$P < 0.0001$. Data are representative of three independent experiments.

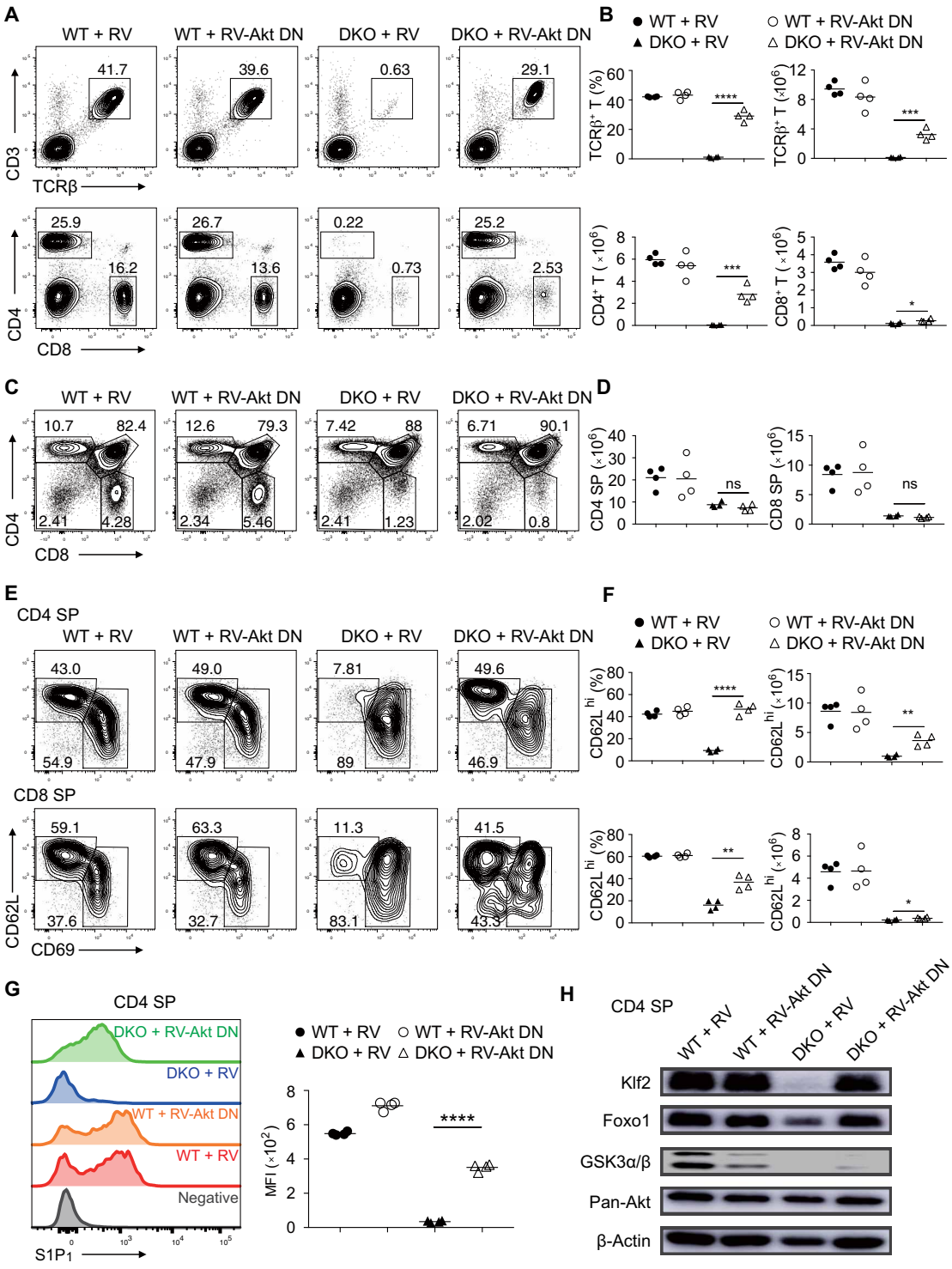

Fig. 5. Suppression of Akt signaling restores the egress of GSK3-deficient thymocytes. (**A**) Flow cytometry analysis of $CD3^+TCR\beta^+$ (top), $CD4^+$, and $CD8^+$ (bottom) T cells in the lymph nodes of recipient mice reconstituted with WT and DKO bone marrow cells transduced with empty retroviruses (RVs) or retroviruses encoding dominant negative Akt (RV-Akt DN). (**B**) Summary of the percentage and number of $CD3^+TCR\beta^+$ (top), $CD4^+$, and $CD8^+$ T cells (bottom) in (A) ($n \geq 3$ per group). (**C**) Flow cytometry analysis of thymocyte development in the recipients in (A). (**D**) Summary of the numbers of CD4 and CD8 SP thymocytes in (C). (**E**) Flow cytometry analysis of $CD62L^{hi}CD69^{lo}$, $CD62L^{lo}CD69^{hi}$ CD4 (top), and CD8 (bottom) SP thymocytes in the recipients in (A). (**F**) Summary of the percentage and number of $CD62L^{hi}CD69^{lo}$ CD4 and CD8 SP thymocytes in (E). (**G**) $S1P_1$ expression on $CD62L^{hi}CD69^{lo}$ CD4 SP thymocytes in the recipients in (A) was analyzed by flow cytometry. $CD62L^{lo}CD69^{hi}$ cells as a negative control (gray). Right: MFI of $S1P_1$ expression on $CD62L^{hi}CD69^{lo}$ CD4 SP thymocytes of indicated groups. (**H**) Immunoblot analysis of Klf2, Foxo1, GSK3α/β, Akt, and β-actin in CD4 SP thymocytes from indicated groups. Each symbol represents an individual mouse. Small horizontal lines indicate the mean (± SEM). $^*P < 0.1$; $^{**}P < 0.01$; $^{***}P < 0.001$; $^{****}P < 0.0001$. Data are representative of two independent experiments.

of *Gsk3a*$^{-/-}$*b*$^{-/-}$ CD4 SP thymocytes (fig. S11, C to E). The expression levels of Klf2 and Foxo1 were also largely restored by Akt DN expression in *Gsk3a*$^{-/-}$*b*$^{-/-}$ thymocytes (Fig. 5H). These results demonstrated that restraining Akt activity in GSK3-deficient thymocytes can largely rescue their egress defect, suggesting that GSK3 controls thymocyte egress mainly by attenuating Akt activity.

mTOR complex 2 (mTORC2) phosphorylates Akt at serine-473, and this plays an important role in Akt activation. Previous studies found that GSK3 directly associates with and phosphorylates Rictor, an essential component of mTORC2, causing the degradation of Rictor and preventing the binding of Akt to mTORC2 (*42*, *43*). We found elevated Ser^{473} phosphorylation of Akt in SDF1-stimulated GSK3-deficient SP thymocytes (Fig. 3G), indicating increased mTORC2 signaling in these cells. Therefore, it is possible that the GSK3 deficiency either stabilizes Rictor and mTORC2 or enhances Akt interaction with mTORC2, leading to elevated Akt activity. To investigate this possibility, we asked whether inhibiting mTORC2 signaling would restore thymocyte egress in *Gsk3a*$^{-/-}$*b*$^{-/-}$ mice. This was achieved by generating *Gsk3a*$^{-/-}$*b*$^{-/-}$*Rictor*$^{fl/fl}$ mice (*44*), which deleted both the Rictor and GSK3 genes by *CD4*-Cre. As shown in fig. S12, deleting the Rictor gene only slightly increased T cell numbers in the periphery, had almost no effect on thymocyte development, and partially restored CD69 down-regulation, $S1P_1$ up-regulation, and Foxo1 and Klf2 protein levels in SP thymocytes of *Gsk3a*$^{-/-}$*b*$^{-/-}$ mice. Therefore, Rictor and mTORC2 play a limited role in mediating GSK3 control of thymus egress through Akt.

We next asked whether the kinase activity of GSK3 is essential for its regulation of thymocyte egress. *Gsk3a*$^{-/-}$*b*$^{-/-}$ bone marrow cells were transduced with retroviruses encoding two kinase-dead mutants of GSK3β K85R and K85M (*45*, *46*), as well as WT GSK3β, and used to reconstitute *Rag2*$^{-/-}$ mice. T cell numbers in the periphery were almost completely restored by WT GSK3β, accompanied by normal CD69 downregulation, $S1P_1$ upregulation, Foxo1 and KLF2 expression on SP thymocytes. In contrast, retroviral expression of K85R and K85M had no such effect (fig. S13, A to F). In a separate experiment, retroviral expression of WT GSK3β in WT CD4 SP thymocytes inhibited SDF1-induced Akt activation and phosphorylation of Foxo1, while kinase-dead K85R mutant of GSK3β had no effect (fig. S13G). These results demonstrated that the kinase activity of GSK3 is essential for its control of thymocyte egress and regulation of the Akt-Foxo1 signaling pathway in SP thymocytes.

Cytoplasmic accumulation of β-catenin promotes Akt activation

A previous study reported that Akt directly interacts with and phosphorylates β-catenin, leading to accumulation of the latter in the cytoplasm (*47*). Our results showed substantial β-catenin accumulation in *GSK3*-deficient SP thymocytes (Fig. 3, D and E), which may associate with Akt and promote its activation. To test this possibility, WT CD4 SP thymocytes were transduced with retroviruses encoding a stabilized form of β-catenin harboring one amino acid substitution at position 33 (termed Ctnnb1 S33Y, as the *Ctnnb1* gene encodes β-catenin) that prevents its phosphorylation by GSK3 and subsequent degradation (*48*). As shown in Fig. 6A, expression of Ctnnb1 S33Y markedly increased the activating phosphorylation of Akt (at Thr^{308} and Ser^{473}) and decreased Foxo1 expression in SDF1-stimulated CD4 SP thymocytes (Fig. 6A). To elucidate how β-catenin promotes Akt activation, Myc-tagged β-catenin and Flag-tagged Akt were cotransfected into human embryonic kidney (HEK) 293T cells, and their subcellular localization was analyzed by fluorescence microscopy. β-Catenin was localized in both cytoplasm and nucleus and exhibited colocalization with Akt mainly on the plasma membrane (Fig. 6B). The interaction between β-catenin and Akt was confirmed in a coimmunoprecipitation experiment (Fig. 6C). We next examined the effect of β-catenin accumulation on the expression of Akt kinases and phosphatases and their interactions with Akt. As shown in fig. S14, expression of stabilized β-catenin (Ctnnb1 S33Y) did not affect the expression and activation of PI3K and PDK1, as well as the expression of Akt phosphatases, PHLPP2, and PP2A (fig. S14). In addition, Ctnnb1 S33Y expression did not affect the interaction between Akt and PI3K-p110α but reduced Akt interaction with RICTOR and slightly decreased Akt interaction with PDK1 (Fig. 6D). Ctnnb1 S33Y expression reduced the association of Akt with its phosphatases PHLPP2 and PP2A (Fig. 6D), suggesting that β-catenin–mediated Akt activation is mainly caused by decreased interactions between Akt and its phosphatases, which results in dampened Akt dephosphorylation and therefore sustained Akt activation.

To further assess the effect of β-catenin accumulation on Akt activation, mouse embryonic fibroblasts (MEFs) were transfected with Ctnnb1 S33Y, subjected to serum starvation for 16 hours to minimize the basal levels of Akt activation, and then restimulated with 0.5% serum to induce Akt activation by growth factors. As shown in Fig. 6E, Ctnnb1 S33Y expression significantly increased Akt activation, as well as Foxo1 phosphorylation and degradation. In both CD4 SP thymocytes and MEFs, β-catenin accumulation was sufficient to promote Akt phosphorylation and Foxo1 degradation in the absence of SDF1 and serum stimulation, respectively (Fig. 6, A and E), suggesting the existence of a tonic β-catenin–Akt-Foxo1 signaling pathway.

We next investigated the cellular compartment where β-catenin activation of Akt occurs. Our results showed that β-catenin was localized in both the cytoplasm and nucleus of HEK293T cells, but predominantly in the cytoplasm of MEFs and *Gsk3a*$^{-/-}$*b*$^{-/-}$ SP thymocytes (Fig. 6, B, E, and F). As the colocalization of β-catenin and Akt was mainly found on the plasma membrane of HEK293T cells (Fig. 6B), we tested whether a membrane-localized β-catenin was sufficient to promote Akt activation. A myristoylation tag was inserted at the N terminus of Ctnnb1 S33Y (termed Myr-Ctnnb1 S33Y) to target β-catenin to the plasma membrane and endomembranes. As shown in (Fig. 6, G and H), Myr-Ctnnb1 S33Y was successfully localized to membranes in the cytoplasm and excluded from the nucleus and was capable of promoting Akt activation and Foxo1 degradation as much as Ctnnb1 S33Y. Therefore, these results showed that in the absence of GSK3, β-catenin accumulates in the cytoplasm, where it interacts with and promotes the activation of Akt.

Ctnnb1 deletion restores emigration of GSK3-deficient thymocytes

Next, we asked whether β-catenin accumulation causes thymic retention of GSK3-deficient thymocytes. To answer this question, *Gsk3a*$^{-/-}$*b*$^{-/-}$ mice were crossed with *Ctnnb1*$^{fl/fl}$ mice to generate *Gsk3a*$^{-/-}$*b*$^{-/-}$*Ctnnb1*$^{fl/fl}$ mice. The results showed that the percentage and number of T cells in the spleen and peripheral lymph nodes were restored to WT levels in *Gsk3a*$^{-/-}$*b*$^{-/-}$*Ctnnb1*$^{fl/fl}$ mice (Fig. 7, A and B, and fig. S15, A and B). *Ctnnb1* deletion significantly rescued the frequency and number (Fig. 7, C and D), CD62L up-regulation and

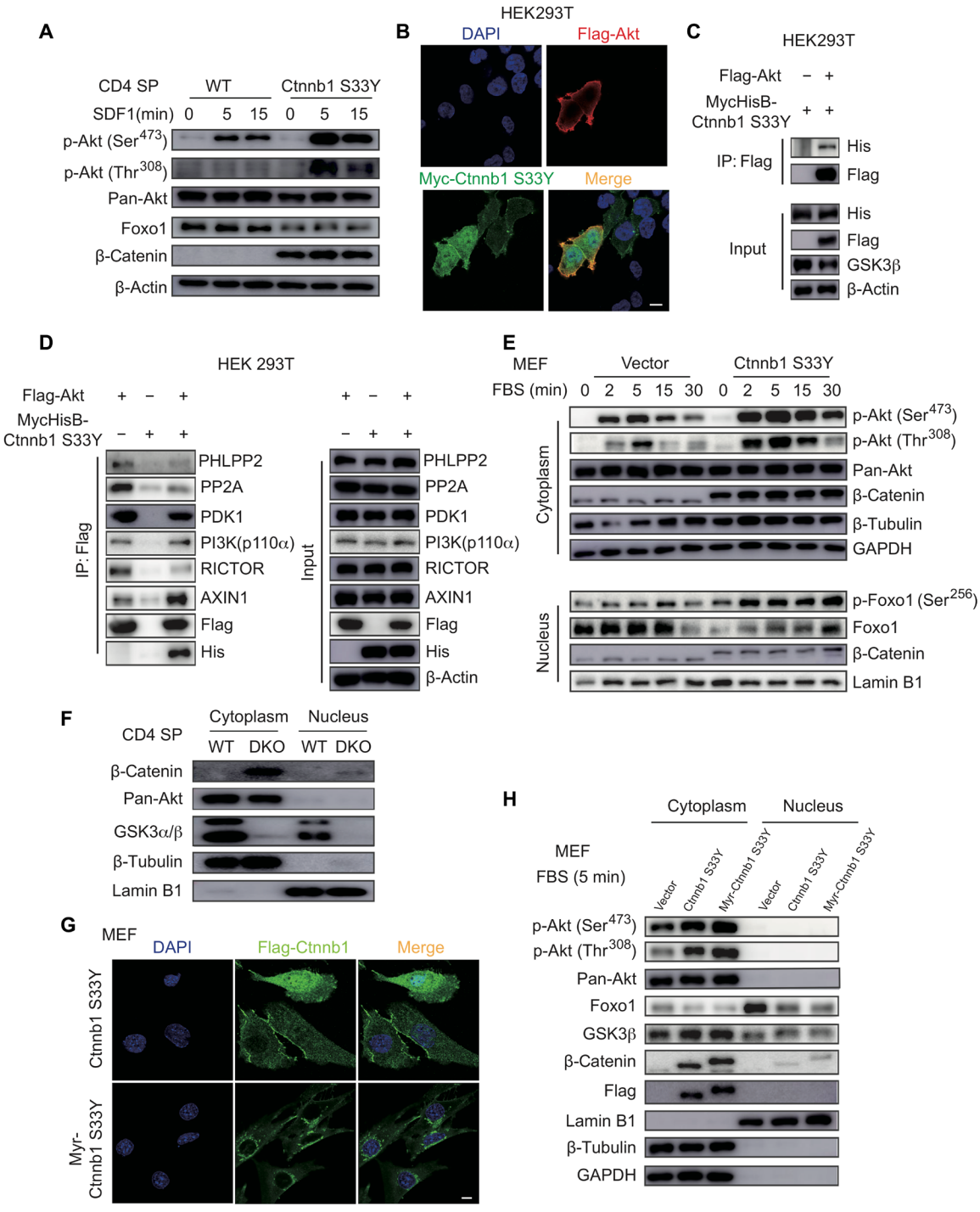

Fig. 6. Stabilized β-catenin promotes Akt activation. (**A**) Immunoblot analysis of phospho-Akt, pan-Akt, Foxo1, β-catenin, and β-actin in WT and stabilized β-catenin (Ctnnb1 S33Y)–transduced CD4 SP thymocytes stimulated with SDF1 for indicated amounts of time. (**B**) Representative immunofluorescence images of 293T cells transfected with Flag-Akt and Myc-Ctnnb1 S33Y and stained for Akt (red), β-catenin (green), and 4′,6-diamidino-2-phenylindole (DAPI; blue, nuclear staining). Scale bars, 10 μm. (**C** and **D**) 293T cells were transfected with MycHis-Ctnnb1 S33Y and/or Flag-Akt. Total cell lysates were immunoprecipitated with Flag antibody and analyzed by immunoblotting with indicated antibodies. (**E**) Mouse embryonic fibroblasts (MEFs) were transduced with lentiviruses encoding β-catenin S33Y (Ctnnb1 S33Y) or vector, serum-starved for 16 hours, and restimulated with 0.5% FBS for indicated amounts of time. Cytoplasmic and nuclear fractions were analyzed by immunoblotting with indicated antibodies. (**F**) Immunoblot analysis of cytoplasmic and nuclear fractions of CD4 SP thymocytes from WT and DKO mice. (**G**) MEFs were transduced with lentiviruses encoding β-catenin S33Y (Ctnnb1 S33Y) or myristoylation-tagged β-catenin S33Y (Myr-Ctnnb1 S33Y), serum-starved for 16 hours, restimulated with 0.5% FBS for 5 min, and analyzed by immunofluorescence staining for β-catenin S33Y (green) and DAPI (blue, nuclear staining). Scale bar, 10 μm. (**H**) Immunoblot analysis of cytoplasmic and nuclear fractions of MEFs from (G). Data are representative of at least two (D) and three (A to C and E to H) independent experiments.

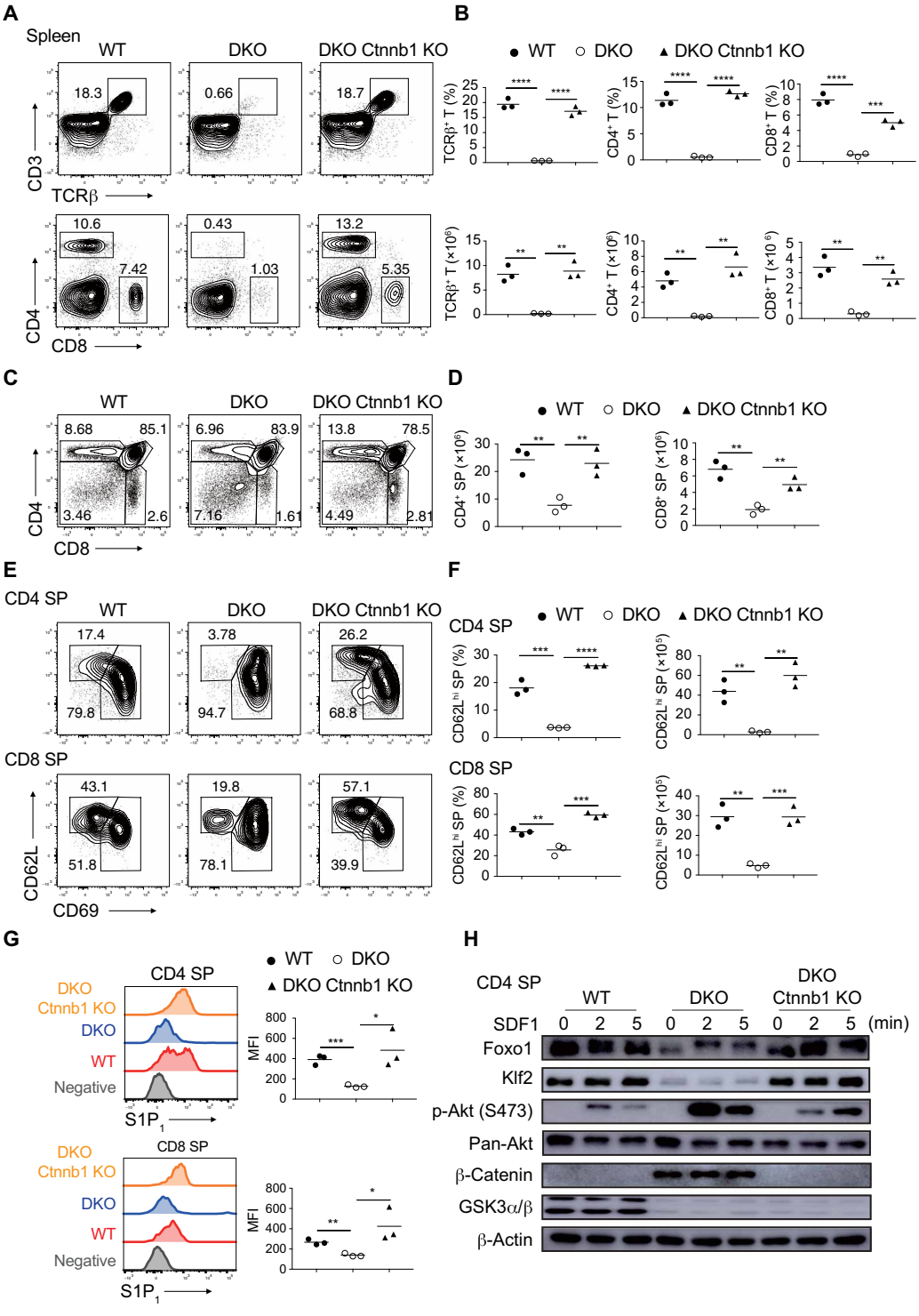

Fig. 7. *Ctnnb1* deletion restores the egress of GSK3-deficient thymocytes. (**A**) Flow cytometry analysis of $CD3^+TCR\beta^+$ (top), $CD4^+$, and $CD8^+$ T (bottom) cells in the spleen of 4- to 6-week-old WT, DKO, and *Gsk3a*$^{-/-}$*b*$^{-/-}$*Ctnnb1*$^{-/-}$ (DKO Ctnnb1 KO) mice. (**B**) Summary of the percentage (top) and number (bottom) of $CD3^+TCR\beta^+$, $CD4^+$, and $CD8^+$ T cells in (A) ($n = 3$ per group). (**C**) Flow cytometry analysis of thymocyte development in mice in (A). (**D**) Summary of numbers of CD4 and CD8 SP thymocyte in (C). (**E**) Flow cytometry analysis of $CD62L^{hi}CD69^{lo}$ cells among CD4 (top) and CD8 (bottom) SP thymocytes in mice in (A). (**F**) Summary of the percentage and number of $CD62L^{hi}CD69^{lo}$ cells among CD4 and CD8 SP cells in (E). (**G**) $S1P_1$ expression on $CD62L^{hi}CD69^{lo}$ CD4 (top) and CD8 (bottom) SP thymocytes in mice in (A) was analyzed by flow cytometry. $CD62L^{lo}CD69^{hi}$ cells as a negative control (gray). Right: MFI of $S1P_1$ expression on $CD62L^{hi}CD69^{lo}$ CD4 and CD8 SP thymocytes of indicated genotypes. (**H**) Immunoblot analysis of the Akt-Foxo1-Klf2 pathway in CD4 SP thymocytes stimulated with SDF1 for indicated amounts of time. Each symbol represents an individual mouse. Small horizontal lines indicate the mean (± SEM). *$P < 0.1$; **$P < 0.01$; ***$P < 0.001$; ****$P < 0.0001$. Data are representative of at least three independent experiments.

CD69 down-regulation (Fig. 7, E and F), S1P- and CCL19-induced migration (fig. S15G), and the expression of $S1P_1$, CCR7, and CXCR4 of *Gsk3a*$^{-/-}$*b*$^{-/-}$ SP thymocytes (Fig. 7G and fig. S15, C to F). Akt activation and Foxo1 and Klf2 expression were all restored to WT levels in *Gsk3a*$^{-/-}$*b*$^{-/-}$*Ctnnb1*$^{fl/fl}$ SP thymocytes (Fig. 7H). Together, these results demonstrated that GSK3 drives thymocyte egress mainly by preventing β-catenin accumulation and Akt activation (Fig. 8).

DISCUSSION

This study identifies GSK3 as a key driver of thymocyte egress. On the basis of our results, we propose the following model. Immediately after the initiation of positive selection, DP thymocytes up-regulate CD69 and CCR7. While CD69 prevents premature emigration of DP and SP thymocytes from the thymus by inducing the internalization and degradation of $S1P_1$, CCR7 promotes the migration of thymocytes to the medulla and facilitates their scanning of mTECs and dendritic cells for self-peptide–MHC complexes (*1*, *2*). The fate of SP thymocytes in the medulla is determined by three intertwining forces. The dominant force is strong TCR signaling triggered by self-peptide–MHC complexes derived from tissue-specific antigens, which leads to the death of SP thymocytes (negative selection) or their differentiation into agonist selection lineages (*4*). The second force, which we term tonic signaling (*36*, *37*), is much weaker, including residual TCR signaling initiated by positive selection, signaling triggered by TCR engagement of self-peptide–MHC complexes with low affinity, and signaling emanated from receptors for cytokines and chemokines produced by medullary stromal cells (*1*). Those tonic signals, if left unchecked, can be amplified by β-catenin through its association with and activation of Akt, leading to Foxo1 phosphorylation and degradation, down-regulation of Klf2 and $S1P_1$ expression, and retention of thymocytes in the thymus. GSK3 represents the third force, which, through its constitutive expression and activity, suppresses β-catenin activation of Akt and drives thymocyte egress. Therefore, the constitutive expression of GSK3 represents a default pathway that drives emigration of SP thymocytes from the thymus.

Our findings reveal a novel signaling pathway mediated by GSK3. Through complex formation with distinct signaling components, GSK3 participates in different signaling pathways, most notably the Wnt–β-catenin pathway. Similar to GSK3, β-catenin is constitutively expressed in many cells. In the absence of Wnt signaling, β-catenin attaches to cadherins and α-catenin at the cell membrane adherens junctions, where it functions as an integral structural component. The remaining β-catenin forms a complex with scaffolding proteins Axin and APC, where it is phosphorylated by GSK3 at multiple serine and threonine residues in the N terminus and subsequently degraded through the ubiquitination-proteasome pathway. Upon Wnt signaling, Dishevelled protein is recruited to the Axin complex to inhibit GSK3, resulting in cytoplasmic accumulation and subsequent nuclear translocation of β-catenin, where it associates with transcription factors TCF1 and LEF1 and transactivates Wnt target genes (*49*). As adherens junctions do not exist in thymocytes, all β-catenin proteins are subjected to regulation by GSK3, which, due to constitutive expression and activity of GSK3, results in a complete degradation of β-catenin. The critical importance of GSK3-driven β-catenin degradation came to light only when both *GSK3α* and *GSK3β* genes were ablated, leading to β-catenin accumulation, Akt activation, and thymocyte retention in the thymus. That β-catenin accumulated predominantly in the cytoplasm of *GSK3*-deficient thymocytes and that a myristoylated form of β-catenin, which is excluded from the nucleus, was sufficient to promote Akt activation suggest the existence of a novel GSK3–β-catenin–Akt signaling pathway that is independent of the transcriptional activation function of β-catenin. Further molecular analysis showed that β-catenin interrupted the interaction between Akt and its phosphatases PHLPPL and PP2A, resulting in dampened Akt dephosphorylation and sustained Akt activation.

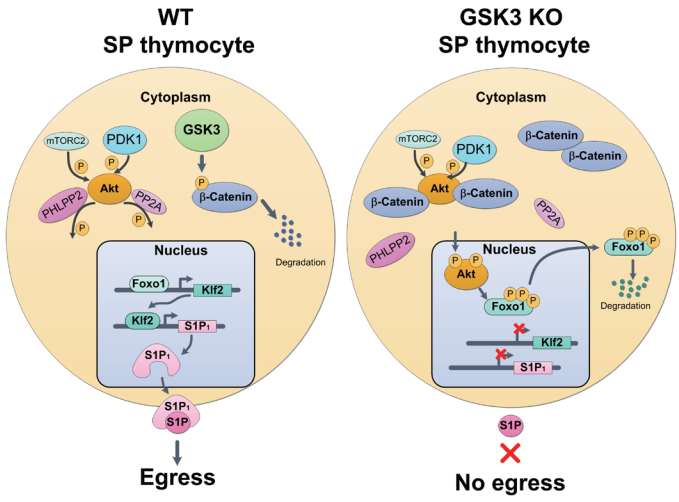

Fig. 8. GSK3 regulation of thymocyte egress: A model. The S1P gradient provides a driving force for the egress of mature thymocytes into the bloodstream. A Foxo1-Klf2 axis controls the expression of S1P receptor $S1P_1$ on mature thymocytes. Constitutive expression and activity of GSK3 in WT thymocytes are required for suppressing tonic Akt signaling by phosphorylating β-catenin, leading to its degradation. In the absence of GSK3, β-catenin accumulates in the cytoplasm, where it promotes Akt activation by decreasing the association of Akt with its phosphatases, PHLPP2 and PP2A, resulting in Foxo1 phosphorylation and degradation, diminished Klf2 and $S1P_1$ expression, and impaired thymocyte egress.

That GSK3 exerts its function in thymocyte egress by suppressing a β-catenin–Akt signaling pathway is further supported by the remarkable similarity in phenotypes caused by GSK3 deletion, β-catenin stabilization, Pten deletion, and Akt activation. Previous studies found that *Lck-Cre*–mediated deletion of the *Pten* gene allowed the generation of DP thymocytes in the absence of RAG2 (*50*) and impaired the emigration of mature thymocyte from the thymus (*51*) and that all *Pten*$^{fl/fl}$*Lck-Cre* mice died of T cell lymphomas within 17 weeks (*52*). Transgenic expression of a constitutively active Akt gene driven by the proximal *Lck* promoter also allowed the generation of DP thymocytes in the absence of RAG2 and led to the development of T cell lymphomas in most of the transgenic mice (*53*, *54*). Similarly, *Lck-Cre*–mediated deletion of exon 3 of the *Ctnnb1* gene, which resulted in β-catenin stabilization and accumulation, allowed thymocyte development to DP and SP stages in the absence of RAG2. Half of the mutant mice succumbed to thymic lymphomas in 20 weeks (*55*, *56*).

In addition to controlling thymocyte egress, GSK3 also controls the survival, cell size, and proliferation of SP thymocytes. In the absence of GSK3, SP thymocytes showed significant increases in cell size and proliferation and were more susceptible to apoptosis. This is reminiscent of a recent study reporting that GSK3 controlled cell

size, proliferation, and survival of B cells (*23*). We speculate that elevated Akt signaling underlies these cellular phenotypes of GSK3-deficient SP thymocytes and B cells. As Cre recombinase expression is turned on in preselection DP thymocytes in the *Cd4*-Cre mice (*21*), elevated Akt signaling may affect negative selection of SP thymocytes by causing the death of some T cell clones that would have survived in WT mice, resulting in a reduction in the numbers of SP thymocytes in $Gsk3a^{-/-}b^{-/-}$ mice. Introducing the P14 TCR transgene into $Gsk3a^{-/-}b^{-/-}$ mice completely restored the numbers of DP and CD8 SP thymocytes, suggesting that GSK3 controls the threshold of negative selection of SP thymocytes. Therefore, the reduction in the numbers of SP thymocytes in $Gsk3a^{-/-}b^{-/-}$ mice may be caused by increased apoptosis and enhanced negative selection of these cells.

This study provides fresh insights into the well-established relationship between the Wnt–β-catenin pathway and cancer. Mutations in this pathway have been found in a broad spectrum of human cancers. In all these cases, the common denominator is the accumulation of β-catenin in cancer cells (*57*). It has been thought that transcriptional activation of TCF/LEF target genes by nuclear β-catenin causes cancer. The phenotype of $TCF1^{-/-}$ mice suggested that additional mechanisms may exist. $TCF1^{-/-}$ mice developed adenomas in the gut and mammary glands. Crossing $TCF1^{-/-}$ mice with cancer-prone $Apc^{Min/+}$ mice resulted in an offspring with 10 times the number of intestinal polyps relative to $Apc^{Min/+}$ littermates (*58*), suggesting that TCF1 is a tumor suppressor, that genetic ablation of TCF1 could independently contribute to cancer, and that loss-of-function mutations of TCF1 could synergize with mutations of other genes in the Wnt–β-catenin pathway to drive cancer progression. Findings from our study show that cytoplasmic accumulation of β-catenin promotes Akt activation, which is oncogenic in its own right. It is also conceivable that β-catenin–Akt signaling synergizes with transcriptional activation of TCF/LEF target genes by β-catenin to drive cancer development. Future investigation of the role of β-catenin–Akt signaling in cancer will facilitate the design of better strategies targeting aberrant Wnt–β-catenin signaling for cancer therapy.

MATERIALS AND METHODS

Mice

The generation of $Gsk3a^{fl/fl}$, $Gsk3b^{fl/fl}$, $Rictor^{fl/fl}$, *Rosa26-flox-STOP-FOXO1AAA* (*Foxo1AAA*), $Ctnnb1^{fl/fl}$ (Jax stock 022775), *CD4-Cre* (Jax stock 017336), $CD45.1^{+}$ *B6.SJL* (Jax stock 002014), *P14*, *OT-II*, $Rag2^{-/-}$ (Jax stock 008449), and *B6.PL-Thy1a/CyJ* (Jax stock 000406) mice was previously reported (*19*, *20*, *31*, *32*, *39*, *44*, *59*–*61*). Unless otherwise noted, $Gsk3a^{fl/fl}Gsk3b^{fl/fl}$*Cd4*-Cre mice were analyzed at 4 to 6 weeks of age, while other mice were used as donors or recipients at 8 to 12 weeks of age. All mice were bred and housed under specific pathogen–free conditions. All animal experiments were approved by the Animal Care and Use Committee of Xiamen University.

Antibodies and reagents

Anti-CD3 (145-2C11), anti-CD4 (GK1.5 or RM4-5), anti-CD8α (53-6.7), anti-CD5 (53-7.3), anti-CD24 (M1/69), anti-CD25 (PC61.5), anti-CD44 (IM7), anti-CD62L (MEL-14), anti-CD69 (H1.2F3), anti-CD45.1 (A20), anti-CD45.2 (104), anti-B220 (RA3-6B2), anti-Thy1.2 (53-2.1), anti-Qa2 (69H1-9-9), anti-CCR7 (4B12), anti-CXCR4 (2B11), streptavidin-APC, anti–IL-7R (A7R34), and annexin V (11-8005-74) were from eBioscience. Anti-Thy1.1 (OX-7), anti-TCRβ (H57-597), anti–β7-integrin (FIB504), biotin-conjugated antibody to rat immunoglobulin G2a (IgG2a; MR G2a-83), and anti–Bcl-2 (Bcl/10C4) were from BioLegend. Rat anti-mouse S1P1/EDG-1 (S1PR1) monoclonal IgG2a antibody (MAB7089) and recombinant mouse SDF1α were from R&D Systems. Anti-PTEN (138G6), antibody to Akt phosphorylated at Ser^{473} (D9E) or Thr^{308} (244F9), antibody to Foxo1 phosphorylated at Ser^{256} (#9461), antibody to PI3K phosphorylated at p85 (Tyr^{458})/p55 (Tyr^{199}) (#4288), anti-GSK3α (D80D1), anti-GSK3β (3D10), anti-GSK3α/β (D75D3), anti–pan-Akt (C67E7), anti-FoxO1 (C29H4), anti-Rictor (53A2), anti-Foxo3a (75D8), anti–β-catenin (D10A8), antibody to β-catenin phosphorylated at Ser^{552} (#9566), anti–PP2A C subunit (#2038), anti-PI3K p110α (C73F8), anti-PDK1 (D37A7), and DYKDDDDK tag (D6W5B) were from Cell Signaling Technology. Anti-Klf2 (09-820) and horseradish peroxidase (HRP)–conjugated goat anti-rabbit and goat anti-mouse were from Merck Millipore. Anti–β-actin (66009-1-Ig), anti–β-tubulin (66240-1-Ig), anti–lamin B1 (66095-1-Ig), and 6*His,His-Tag antibody (66005-1-Ig) were from Proteintech. Anti–c-Myc (9E10) was from Santa Cruz Biotechnology. Rabbit anti-PHLPPL (A300-661) was from Bethyl. Antibody to PDK1 phosphorylated at S241 (AP0426) was from ABclonal. Recombinant murine IL-7, IL-3, IL-6, and stem cell factor 1 (SCF1) were from PeproTech. 5-Bromo-2′-deoxyuridine (BrdU; 559619) and the Active Caspase-3 Apoptosis Kit (550914) were from BD Biosciences. FLAG M2 Affinity Gel (A2220) was from Sigma-Aldrich. Pierce Protein A/G Agarose (#20422) was from Thermo Fisher Scientific.

Plasmid constructs

For mammalian cell expression, full-length complementary DNA (cDNA) of Gsk3β was polymerase chain reaction (PCR)–amplified from mouse cDNA. For retroviral transduction of mouse CD4 SP thymocytes and bone marrow reconstitution, genes encoding WT Gsk3β and Gsk3β (S9A) were cloned into an MSCV retroviral vector containing internal ribosomal entry site (IRES)–Thy1.1 (RV). Genes encoding WT Gsk3β, Gsk3β (K85R), and Gsk3β (K85M) were inserted into an MSCV retroviral vector expressing green fluorescent protein (GFP). The QuikChange II Site-Directed Mutagenesis Kit was used to generate Gsk3β mutations (S9A, K85R, and K85M) following the manufacturer's instructions (Agilent Technologies). RV-Akt DN was provided by H. Chi (St. Jude Children's Research Hospital) (*41*). Plasmid encoding stabilized β-catenin (Ctnnb1 S33Y) was a gift from B.-A. Li (Xiamen University). Ctnnb1 S33Y cDNA was subcloned into a lentiviral vector pLV-C-3Flag-IRES-GFP and pEF4-C-MycHisB. Myr-Ctnnb1 S33Y was generated by adding a myristoylation tag (MGSSKSKPKDPSQ) and a $GGGS_3$ linker at the N terminus of Ctnnb1 S33Y. To generate Myr-Ctnnb1 S33Y cDNA, primer sequence designed for annealing and ligation into Ctnnb1 S33Y–expressing vector is shown as follows: 5′-ATG-GGGAGTAGCAAGAGCAAGCCTAAGGACCCCAGCCAGG-GTGGCGGTTCCGGCGGTGGCTCGGGAGGTGGCTCA-3′. Mouse Akt1 was inserted into pCDNA6.0-C-Flag. All plasmids were verified by DNA sequencing.

Mixed bone marrow chimeras

$Rag2^{-/-}$ mice were irradiated with a sublethal dose of 5.5 Gy in an RS-2000 irradiator (Rad Source). Bone marrow cells from WT B6 (on a CD45.1, CD45.1/2, or Thy1.1 genetic background) and DKO

(on a CD45.2 and Thy1.2 genetic background) mice were subjected to red blood cell lysis and T cell depletion by magnetic separation, mixed in a 1:1 ratio (5×10^6 to 10×10^6 cells in total), and adoptively transferred into irradiated recipients by intravenous injection. All recipients were analyzed 6 to 8 weeks after reconstitution.

Adoptive transfer

WT (on a CD45.1 or Thy1.1 genetic background) and DKO (on a CD45.2 and Thy1.2 genetic background) CD4 SP mature thymocytes were sorted by flow cytometry, mixed in a 1:1 ratio, and intravenously injected into WT recipients (on a Thy1.1 or CD45.1 genetic background). Alternatively, WT, DKO, and DKO;Foxo1AAA (all CD45.2 background) $TCR\beta^+CD4^+$ SP mature thymocytes were separately injected into CD45.1 WT recipients. One day after injection, lymph node cells were collected and analyzed by flow cytometry.

Intrathymic injection

Intrathymic FITC injection was performed as previously described (*62*). Briefly, mice were anesthetized, and the muscle layer between trachea and clavicle was dissociated carefully to expose the thymus. A Hamilton syringe was used to inject 10 μl of FITC solution [1 μg/μl in phosphate-buffered saline (PBS), Thermo Fisher Scientific], followed by suturing the wound using autoclips. Mice were recovered under a heating lamp. One day after injection, cells in the peripheral blood, spleen, and lymph nodes were examined for FITC incorporation. The percentage of FITC-labeled $CD4^+$ or $CD8^+$ T cells in the spleen or lymph nodes was calculated as total number of FITC-labeled $CD4^+$ or $CD8^+$ T cells in these organs divided by total ($CD4^+$ or $CD8^+$ SP thymocytes plus $CD4^+$ or $CD8^+$ T cells in the spleen and lymph nodes) FITC-labeled cells, multiplied by 100. For intrathymic injection of cells, 1 million cells in 10 μl of PBS were injected into the thymus following the same procedure.

BrdU administration and detection

Mice received BrdU (200 μg per mouse) by intraperitoneal injection. Thymocytes were collected at 16 hours after BrdU injection. BrdU incorporation in thymocytes was detected by the FITC-BrdU Flow Kit (BD Biosciences). Briefly, thymocytes were fixed, permeabilized with BD Cytofix/Cytoperm buffer for 30 min after surface staining, treated with deoxyribonuclease I for 15 min at room temperature to expose incorporated BrdU, stained with FITC-conjugated anti-BrdU antibody, and analyzed by flow cytometry.

Flow cytometry

Single-cell suspension was prepared from the spleen, draining lymph nodes, and thymus after red blood cell lysis. For cell surface marker staining, antibodies were combined, added to cells, and incubated for 30 min at 4°C. For surface CCR7 and CXCR4 staining, cells were incubated in complete medium at 37°C for 30 min before staining. After wash with fluorescence-activated cell sorting (FACS) buffer [PBS with 0.5% bovine serum albumin (BSA) and 0.05% NaN_3] once, antibody cocktails were added to cells, incubated at 37°C for 30 min, washed with FACS buffer at room temperature twice, and resuspended with FACS buffer. For S1P1 staining, thymocytes were incubated with rat anti-mouse S1P1 primary antibody for 2 hours at 4°C. After washing twice with magnetic-activated cell sorting (MACS) buffer [PBS containing 2% fetal bovine serum (FBS) and 2 nM EDTA], cells were incubated at 4°C for 30 min with a secondary biotin-labeled anti-rat IgG2a antibody that was preincubated with MACS buffer containing 2% mouse serum for 15 min. After washing twice with MACS buffer, cells were stained with streptavidin-APC for 15 min, followed by addition of rat serum and incubation for 10 min. Cells were washed with MACS buffer once, followed by incubation with other cell surface markers. All FACS-stained samples were kept at 4°C and analyzed at a low speed on a flow cytometer. For intracellular staining of Bcl-2, after cell surface marker staining, cells were fixed and permeabilized for 30 min in the Fix/Perm Buffer (eBioscience). After washing with the perm buffer, cells were blocked with goat serum for 30 min at room temperature and stained with rabbit anti–Bcl-2 or FITC-labeled anti–Bcl-2 for 1 hour. After washing five times, cells were incubated with AF647-labeled anti-rabbit IgG antibody for 30 min at 4°C. BrdU and active caspase-3 staining (BD Biosciences), as well as annexin V staining (eBioscience), were done following the manufacturer's instructions. All flow cytometry data were acquired on Fortessa or LSRFortessa X-20 (BD Biosciences), or a NovoCyte flow cytometer (ACEA Biosciences, Agilent), and analyzed with FlowJo software 10 (Treestar).

Thymocyte stimulation

Sorted cells were rested for 3 hours and washed twice with cold PBS. For SDF1 stimulation, 100 μl of SDF1 solution (100 ng/ml in PBS) was added to cells in a FACS tube (BD) and incubated for 2 or 5 min in a 37°C water bath. Stimulation was terminated by adding ice-cold PBS, followed by cell lysis and immunoblot analysis.

Retroviral transduction

Plat-E packaging cells were transfected with 3 μg of retroviral vector along with polyethylenimine (PEI). At 48 and 72 hours after transfection, retrovirus-containing supernatants were collected and stored at −80°C. CD4 SP mature thymocytes were sorted from WT or GSK3α/β DKO mice and stimulated with anti-CD3 (2 μg/ml) and anti-CD28 (1 μg/ml) in a complete RPMI 1640 medium containing 10% FBS and IL-7 (2 ng/ml). One day later, activated cells were transduced with retrovirus together with polybrene (10 μg/ml) and IL-2 (20 ng/ml) by centrifugation of cells for 60 min at 2000 rpm at 37°C. After infection, cells were harvested and lysed. To adoptively transfer transduced cells into mice, cells were rested in medium with IL-2 (20 ng/ml) for 2 days and then in medium with IL-7 (2 ng/ml) for another day, followed by intravenous injection. For bone marrow reconstitution, mice were pretreated with 5-fluorouracil (Sigma-Aldrich) for 5 days. Bone marrow cells were harvested and cultured in complete Dulbecco's modified Eagle's medium (DMEM) supplemented with 10% FBS containing IL-3 (20 ng/ml), IL-6 (25 ng/ml), and SCF1 (100 ng/ml). Concentrated retroviral supernatants together with polybrene (8 μg/ml) were used for spin infection of cultured bone marrow cells at 2500 rpm, 32°C for 2 hours.

Lentiviral transduction

Lentiviruses were produced by transfecting HEK293T cells with the pLV-C-3Flag-IRES-GFP vector encoding Ctnnb1 S33Y or Myr-Ctnnb1 S33Y with PEI. Viral supernatants were harvested at 48 hours after transfection. MEFs were infected with lentiviruses and polybrene (10 μg/ml) by centrifugation of cells at 1200*g* for 30 min at 37°C. Two days after infection, GFP-positive cells were sorted and β-catenin expression was detected by immunoblot analysis.

Transwell migration assay

The experiment was performed as previously described (*63*). Briefly, 1×10^6 CD4 SP thymocytes in 100 μl of medium were loaded into the upper chamber of a 24-well transwell chemotaxis chamber (Corning). Cells were allowed to migrate to the lower chamber containing either CCL19 (200 ng/ml) or 10 mM S1P for 3 hours. Alternatively, CD4 SP thymocytes were transduced with retroviruses encoding indicated genes, rested for 24 hours in medium containing IL-7 (2 ng/ml), loaded into the upper chamber, and allowed to transmigrate into the lower chamber containing either CCL19 (200 ng/ml; for 3 hours) or 10 mM S1P (for 10 hours). Cells in the lower chamber were counted.

Preparation of nuclear extracts

For sorted CD4 SP thymocytes, cells were rested for 3 hours in complete medium in a 37°C incubator. After resting and washing twice in PBS, 1×10^7 cells were lysed in 500 μl of 0.15% NP-40 lysis buffer (10 mM Hepes, 10 mM KCl, 0.1 mM EDTA, 0.1 mM EGTA, and 0.15% NP-40) for 15 min on ice. The homogenates were centrifuged at a full speed (>12,000*g*) for 3 min, and the supernatant was collected as cytoplasmic extracts. The nuclear pellet was washed three times with 0.15% NP-40 lysis buffer and resuspended in radioimmunoprecipitation assay lysis buffer [25 mM tris-Cl (pH 7.4), 150 mM NaCl, 1 mM EDTA, 1% NP-40, and 5% glycerol], followed by incubation on ice for 30 min with vortexing every 10 min. For HEK293T cells and MEFs, the nuclear pellets were lysed in the Triton X-100 lysis buffer [20 mM tris-HCl (pH 7.5), 150 mM NaCl, 1% Triton X-100, 1 mM EDTA (pH 8.0), 1 mM EGTA (pH 8.0), 2.5 mM NaPiP, 1 mM Na_3VO_4, and 1 mM β-glycerophosphate] supplemented with phosphatase inhibitor cocktail (100×) (phenylmethylsulfonyl fluoride, aprotinin, leupeptin, pepstatin; Sangon Biotech). The lysates were centrifuged at a full speed (>12,000*g*) at 4°C for 10 min. The supernatant was collected as nuclear extracts, aliquoted, and stored at −80°C.

Immunoblot and immunoprecipitation

For immunoblot, sorted CD4 SP and CD8 SP thymocytes, HEK293T cells, and MEFs were rested and lysed in the lysis buffer [20 mM tris-HCl (pH 7.5), 150 mM NaCl, 1% Triton X-100, 1 mM EDTA, and 1 mM EGTA] supplemented with Halt Protease and Phosphatase Inhibitor Cocktail (Thermo Fisher Scientific). Cell lysates were resolved on SDS–polyacrylamide gel electrophoresis gels and transferred to nitrocellulose membranes (Merck Millipore). Primary antibodies were diluted in 1× tris-buffered saline (TBS) [10 mM tris-HCl (pH 8.0) and 150 mM NaCl] with 5% (w/v) BSA or nonfat milk, followed by overnight incubation at 4°C. After washing three times in TBS buffer with 0.5% Tween 20, HRP-conjugated goat anti-rabbit or goat anti-mouse antibody was incubated with the membrane. After washing three times in TBS buffer with 0.5% Tween 20, protein bands were visualized with ECL Select Western Blotting Detection Reagent (GE Healthcare) or Immobilon Western Chemiluminescent HRP Substrate (Merck Millipore) following the manufacturer's instructions (GE Healthcare). Images were acquired with Amersham Imager 600 (GE Healthcare). Immunoprecipitations were performed by using FLAG M2 Affinity Gel following the manufacturer's instructions. Briefly, HEK293T cells were collected and lysed in the lysis buffer [20 mM tris-HCl (pH 7.5), 150 mM NaCl, 1% Triton X-100, 1 mM EDTA, 1 mM EGTA, 2.5 mM sodium pyrophosphate, 1 mM β-glycerophosphate, and 1 mM Na_3VO_4] supplemented with Halt Protease and Phosphatase Inhibitor Cocktail (Thermo Fisher Scientific). Cell lysates were centrifuged at 14,000*g* for 20 min. Protein concentration of supernatants was determined by the BCA Protein Quantification Kit (Yeasen). Supernatants were incubated with FLAG M2 Affinity Gel at 4°C for 16 hours, followed by washing beads four times with lysis buffer. Immunoprecipitated proteins were eluted with 2× SDS loading buffer with 1% β-mercaptoethanol and 3× Flag peptide (3 mg/ml; a gift from J. Han, Xiamen University) by vigorous shaking at 1200 rpm for 25 min on the Mixing Block (ThermoCell) and analyzed by immunoblot.

Immunofluorescence microscopy

HEK293T cells were seeded on coverslips in six-well plates to a 70 to 80% confluence and transfected with plasmids encoding genes of interest. After 36 hours of culture, cells were washed with prewarmed PBS three times and fixed with prewarmed 4% paraformaldehyde for 15 min. The fixed cells were rinsed with PBS three times and permeabilized for 10 min at room temperature with 0.1% Triton X-100 in PBS. After three rinses with PBS, cells were incubated with primary antibodies, and anti-Flag (1:200 dilution; Cell Signaling Technology, rabbit, 14793S) and anti-Myc (1:200 dilution; Cell Signaling Technology, mouse, 2276S) were diluted in PBS with 5% FBS at 4°C overnight. After three rinses with PBS, cells were incubated for 6 to 8 hours with secondary antibodies [1:300; goat anti-rabbit IgG (H+L) Highly Cross-Adsorbed Secondary Antibody, Alexa Fluor 555 (A21429, Thermo Fisher Scientific) and goat anti-mouse IgG (H+L) Highly Cross-Adsorbed Secondary Antibody, Alexa Fluor 647 (A21236, Thermo Fisher Scientific)] at 4°C in the dark. After three rinses with PBS, cells were incubated with 4′,6-diamidino-2-phenylindole (DAPI) diluted in PBS with 5% FBS for 15 min before microscopy analysis. Confocal images were obtained using a Leica TCS SP8 confocal microscope with LAS AF software (Leica, Germany).

RNA sequencing and data analysis

DP, CD4SP, and CD8 SP mature thymocytes were sorted from WT and DKO mice. After resting for 3 hours on ice, total RNA was isolated by Qiagen RNeasy Micro or Mini Kits following the manufacturer's instructions. RNA was quantified with Nano Drops Nucleic Acid Analyzer. One microgram of RNA was used for RNA sequencing with a BGISEQ-500 instrument (BGI, Wuhan). Reads were aligned to the mm10 build of the *Mus musculus* genome with the Hisat2. The alignments were passed to StringTie, which assembled and quantified the transcripts in each sample and generated gene count matrices. Differentially expressed genes were analyzed using DESeq2 package. Genes were considered differentially expressed if they had an adjusted *P* value of 0.01 or less. Differentially expressed genes were analyzed with gene set enrichment analysis (GSEA) and Mouse Genome Database (MGD) (www.informatics.jax.org) to find enriched biological processes and signaling pathways. Heatmaps were generated using the gplots package, with log2(gene count+1). PCA plots were generated using rgl package.

Statistical data analysis

All statistical analyses were performed with Prism7 software (GraphPad). *P* values were determined by using two-tailed Student's *t* tests. Statistical significance is displayed as $*P < 0.05$, $**P < 0.01$, $***P < 0.001$, and $****P < 0.0001$.

SUPPLEMENTARY MATERIALS

Supplementary material for this article is available at https://science.org/doi/10.1126/sciadv.abg6262

View/request a protocol for this paper from *Bio-protocol*.

REFERENCES AND NOTES

1. J. N. Lancaster, Y. Li, L. I. R. Ehrlich, Chemokine-mediated choreography of thymocyte development and selection. *Trends Immunol.* **39**, 86–98 (2018).
2. P. E. Love, A. Bhandoola, Signal integration and crosstalk during thymocyte migration and emigration. *Nat. Rev. Immunol.* **11**, 469–477 (2011).
3. M. A. Weinreich, K. A. Hogquist, Thymic emigration: When and how T cells leave home. *J. Immunol.* **181**, 2265–2270 (2008).
4. G. L. Stritesky, S. C. Jameson, K. A. Hogquist, Selection of self-reactive T cells in the thymus. *Annu. Rev. Immunol.* **30**, 95–114 (2012).
5. M. Matloubian, C. G. Lo, G. Cinamon, M. J. Lesneski, Y. Xu, V. Brinkmann, M. L. Allende, R. L. Proia, J. G. Cyster, Lymphocyte egress from thymus and peripheral lymphoid organs is dependent on S1P receptor 1. *Nature* **427**, 355–360 (2004).
6. R. Pappu, S. R. Schwab, I. Cornelissen, J. P. Pereira, J. B. Regard, Y. Xu, E. Camerer, Y. W. Zheng, Y. Huang, J. G. Cyster, S. R. Coughlin, Promotion of lymphocyte egress into blood and lymph by distinct sources of sphingosine-1-phosphate. *Science* **316**, 295–298 (2007).
7. M. A. Zachariah, J. G. Cyster, Neural crest-derived pericytes promote egress of mature thymocytes at the corticomedullary junction. *Science* **328**, 1129–1135 (2010).
8. J. Zamora-Pineda, A. Kumar, J. H. Suh, M. Zhang, J. D. Saba, Dendritic cell sphingosine-1-phosphate lyase regulates thymic egress. *J. Exp. Med.* **213**, 2773–2791 (2016).
9. M. L. Allende, J. L. Dreier, S. Mandala, R. L. Proia, Expression of the sphingosine 1-phosphate receptor, S1P1, on T-cells controls thymic emigration. *J. Biol. Chem.* **279**, 15396–15401 (2004).
10. P. Cohen, S. Frame, The renaissance of GSK3. *Nat. Rev. Mol. Cell Biol.* **2**, 769–776 (2001).
11. E. Beurel, S. F. Grieco, R. S. Jope, Glycogen synthase kinase-3 (GSK3): Regulation, actions, and diseases. *Pharmacol. Ther.* **148**, 114–131 (2015).
12. P. Patel, J. R. Woodgett, Glycogen synthase kinase 3: A kinase for all pathways? *Curr. Top. Dev. Biol.* **123**, 277–302 (2017).
13. E. Beurel, O. Kaidanovich-Beilin, W. I. Yeh, L. Song, V. Palomo, S. M. Michalek, J. R. Woodgett, L. E. Harrington, H. Eldar-Finkelman, A. Martinez, R. S. Jope, Regulation of Th1 cells and experimental autoimmune encephalomyelitis by glycogen synthase kinase-3. *J. Immunol.* **190**, 5000–5011 (2013).
14. E. Beurel, W. I. Yeh, S. M. Michalek, L. E. Harrington, R. S. Jope, Glycogen synthase kinase-3 is an early determinant in the differentiation of pathogenic Th17 cells. *J. Immunol.* **186**, 1391–1398 (2011).
15. T. Ohteki, M. Parsons, A. Zakarian, R. G. Jones, L. T. Nguyen, J. R. Woodgett, P. S. Ohashi, Negative regulation of T cell proliferation and interleukin 2 production by the serine threonine kinase GSK-3. *J. Exp. Med.* **192**, 99–104 (2000).
16. J. H. Schroeder, L. S. Bell, M. L. Janas, M. Turner, Pharmacological inhibition of glycogen synthase kinase 3 regulates T cell development in vitro. *PLOS ONE* **8**, e58501 (2013).
17. A. Taylor, J. A. Harker, K. Chanthong, P. G. Stevenson, E. I. Zuniga, C. E. Rudd, Glycogen synthase kinase 3 inactivation drives T-bet-mediated downregulation of co-receptor PD-1 to enhance CD8(+) cytolytic T cell responses. *Immunity* **44**, 274–286 (2016).
18. C. W. Tran, S. D. Saibil, T. le Bihan, S. R. Hamilton, K. S. Lang, H. You, A. E. Lin, K. M. Garza, A. R. Elford, K. Tai, M. E. Parsons, K. Wigmore, M. G. Vainberg, J. M. Penninger, J. R. Woodgett, T. W. Mak, P. S. Ohashi, Glycogen synthase kinase-3 modulates Cbl-b and constrains T cell activation. *J. Immunol.* **199**, 4056–4065 (2017).
19. B. W. Doble, S. Patel, G. A. Wood, L. K. Kockeritz, J. R. Woodgett, Functional redundancy of GSK-3α and GSK-3β in Wnt/β-catenin signaling shown by using an allelic series of embryonic stem cell lines. *Dev. Cell* **12**, 957–971 (2007).
20. P. P. Lee, D. R. Fitzpatrick, C. Beard, H. K. Jessup, S. Lehar, K. W. Makar, M. Pérez-Melgosa, M. T. Sweetser, M. S. Schlissel, S. Nguyen, S. R. Cherry, J. H. Tsai, S. M. Tucker, W. M. Weaver, A. Kelso, R. Jaenisch, C. B. Wilson, A critical role for Dnmt1 and DNA methylation in T cell development, function, and survival. *Immunity* **15**, 763–774 (2001).
21. J. Shi, H. T. Petrie, Activation kinetics and off-target effects of thymus-initiated cre transgenes. *PLOS ONE* **7**, e46590 (2012).
22. G. Fu, S. Vallée, V. Rybakin, M. V. McGuire, J. Ampudia, C. Brockmeyer, M. Salek, P. R. Fallen, J. A. H. Hoerter, A. Munshi, Y. H. Huang, J. Hu, H. S. Fox, K. Sauer, O. Acuto, N. R. J. Gascoigne, Themis controls thymocyte selection through regulation of T cell antigen receptor-mediated signaling. *Nat. Immunol.* **10**, 848–856 (2009).
23. J. Jellusova, M. H. Cato, J. R. Apgar, P. Ramezani-Rad, C. R. Leung, C. Chen, A. D. Richardson, E. M. Conner, R. J. Benschop, J. R. Woodgett, R. C. Rickert, Gsk3 is a metabolic checkpoint regulator in B cells. *Nat. Immunol.* **18**, 303–312 (2017).
24. C. D. Surh, J. Sprent, Homeostasis of naive and memory T cells. *Immunity* **29**, 848–862 (2008).
25. M. C. Poznansky, I. T. Olszak, R. H. Evans, Z. Wang, R. B. Foxall, D. P. Olson, K. Weibrecht, A. D. Luster, D. T. Scadden, Thymocyte emigration is mediated by active movement away from stroma-derived factors. *J. Clin. Invest.* **109**, 1101–1110 (2002).
26. F. Vianello, P. Kraft, Y. T. Mok, W. K. Hart, N. White, M. C. Poznansky, A CXCR4-dependent chemorepellent signal contributes to the emigration of mature single-positive CD4 cells from the fetal thymus. *J. Immunol.* **175**, 5115–5125 (2005).
27. Y. Xing, X. Wang, S. C. Jameson, K. A. Hogquist, Late stages of T cell maturation in the thymus involve NF-κB and tonic type I interferon signaling. *Nat. Immunol.* **17**, 565–573 (2016).
28. C. C. Denucci, J. S. Mitchell, Y. Shimizu, Integrin function in T-cell homing to lymphoid and nonlymphoid sites: Getting there and staying there. *Crit. Rev. Immunol.* **29**, 87–109 (2009).
29. B. Ernst, C. D. Surh, J. Sprent, Thymic selection and cell division. *J. Exp. Med.* **182**, 961–971 (1995).
30. C. Pénit, F. Vasseur, Expansion of mature thymocyte subsets before emigration to the periphery. *J. Immunol.* **159**, 4848–4856 (1997).
31. M. J. Barnden, J. Allison, W. R. Heath, F. R. Carbone, Defective TCR expression in transgenic mice constructed using cDNA-based α- and β-chain genes under the control of heterologous regulatory elements. *Immunol. Cell Biol.* **76**, 34–40 (1998).
32. H. Pircher, K. Burki, R. Lang, H. Hengartner, R. M. Zinkernagel, Tolerance induction in double specific T-cell receptor transgenic mice varies with antigen. *Nature* **342**, 559–561 (1989).
33. C. M. Carlson, B. T. Endrizzi, J. Wu, X. Ding, M. A. Weinreich, E. R. Walsh, M. A. Wani, J. B. Lingrel, K. A. Hogquist, S. C. Jameson, Kruppel-like factor 2 regulates thymocyte and T-cell migration. *Nature* **442**, 299–302 (2006).
34. G. T. Hart, K. A. Hogquist, S. C. Jameson, Krüppel-like factors in lymphocyte biology. *J. Immunol.* **188**, 521–526 (2012).
35. A. Eijkelenboom, B. M. Burgering, FOXOs: Signalling integrators for homeostasis maintenance. *Nat. Rev. Mol. Cell Biol.* **14**, 83–97 (2013).
36. N. Garbi, G. J. Hammerling, H. C. Probst, M. van den Broek, Tonic T cell signalling and T cell tolerance as opposite effects of self-recognition on dendritic cells. *Curr. Opin. Immunol.* **22**, 601–608 (2010).
37. D. R. Myers, J. Zikherman, J. P. Roose, Tonic signals: Why do lymphocytes bother? *Trends Immunol.* **38**, 844–857 (2017).
38. Y. M. Kerdiles, D. R. Beisner, R. Tinoco, A. S. Dejean, D. H. Castrillon, R. A. DePinho, S. M. Hedrick, Foxo1 links homing and survival of naive T cells by regulating L-selectin, CCR7 and interleukin 7 receptor. *Nat. Immunol.* **10**, 176–184 (2009).
39. W. Ouyang, W. Liao, C. T. Luo, N. Yin, M. Huse, M. V. Kim, M. Peng, P. Chan, Q. Ma, Y. Mo, D. Meijer, K. Zhao, A. Y. Rudensky, G. Atwal, M. Q. Zhang, M. O. Li, Novel Foxo1-dependent transcriptional programs control T(reg) cell function. *Nature* **491**, 554–559 (2012).
40. R. H. Newton, S. Shrestha, J. M. Sullivan, K. B. Yates, E. B. Compeer, N. Ron-Harel, B. R. Blazar, S. J. Bensinger, W. N. Haining, M. L. Dustin, D. J. Campbell, H. Chi, L. A. Turka, Maintenance of CD4 T cell fitness through regulation of Foxo1. *Nat. Immunol.* **19**, 838–848 (2018).
41. G. Liu, S. Burns, G. Huang, K. Boyd, R. L. Proia, R. A. Flavell, H. Chi, The receptor S1P1 overrides regulatory T cell-mediated immune suppression through Akt-mTOR. *Nat. Immunol.* **10**, 769–777 (2009).
42. C. H. Chen, T. Shaikenov, T. R. Peterson, R. Aimbetov, A. K. Bissenbaev, S.-W. Lee, J. Wu, H.-K. Lin, D. D. Sarbassov, ER stress inhibits mTORC2 and Akt signaling through GSK-3β–mediated phosphorylation of rictor. *Sci. Signal.* **4**, ra10 (2011).
43. J. Koo, X. Wu, Z. Mao, F. R. Khuri, S. Y. Sun, Rictor undergoes glycogen synthase kinase 3 (GSK3)-dependent, FBXW7-mediated ubiquitination and proteasomal degradation. *J. Biol. Chem.* **290**, 14120–14129 (2015).
44. J. A. Magee, T. Ikenoue, D. Nakada, J. Y. Lee, K. L. Guan, S. J. Morrison, Temporal changes in PTEN and mTORC2 regulation of hematopoietic stem cell self-renewal and leukemia suppression. *Cell Stem Cell* **11**, 415–428 (2012).
45. N. Le Floch, C. Rivat, O. De Wever, E. Bruyneel, M. Mareel, T. Dale, C. Gespach, The proinvasive activity of Wnt-2 is mediated through a noncanonical Wnt pathway coupled to GSK-3β and c-Jun/AP-1 signaling. *FASEB J.* **19**, 144–146 (2005).
46. Y. Zhang, W. J. Qiu, D. X. Liu, S. Y. Neo, X. He, S. C. Lin, Differential molecular assemblies underlie the dual function of Axin in modulating the WNT and JNK pathways. *J. Biol. Chem.* **276**, 32152–32159 (2001).
47. Q. Tian, M. C. Feetham, W. A. Tao, X. C. He, L. Li, R. Aebersold, L. Hood, Proteomic analysis identifies that 14-3-3ζ interacts with β-catenin and facilitates its activation by Akt. *Proc. Natl. Acad. Sci. U.S.A.* **101**, 15370–15375 (2004).
48. P. J. Morin, A. B. Sparks, V. Korinek, N. Barker, H. Clevers, B. Vogelstein, K. W. Kinzler, Activation of β-catenin-Tcf signaling in colon cancer by mutations in β-catenin or APC. *Science* **275**, 1787–1790 (1997).
49. M. van de Wetering, W. de Lau, H. Clevers, WNT signaling and lymphocyte development. *Cell* **109**, S13–S19 (2002).

50. T. J. Hagenbeek, M. Naspetti, F. Malergue, F. Garçon, J. A. Nunès, K. B. J. M. Cleutjens, J. Trapman, P. Krimpenfort, H. Spits, The loss of PTEN allows TCR αβ lineage thymocytes to bypass IL-7 and pre-TCR–mediated signaling. *J. Exp. Med.* **200**, 883–894 (2004).
51. L. V. Sinclair, D. Finlay, C. Feijoo, G. H. Cornish, A. Gray, A. Ager, K. Okkenhaug, T. J. Hagenbeek, H. Spits, D. A. Cantrell, Phosphatidylinositol-3-OH kinase and nutrient-sensing mTOR pathways control T lymphocyte trafficking. *Nat. Immunol.* **9**, 513–521 (2008).
52. A. Suzuki, M. T. Yamaguchi, T. Ohteki, T. Sasaki, T. Kaisho, Y. Kimura, R. Yoshida, A. Wakeham, T. Higuchi, M. Fukumoto, T. Tsubata, P. S. Ohashi, S. Koyasu, J. M. Penninger, T. Nakano, T. W. Mak, T cell-specific loss of Pten leads to defects in central and peripheral tolerance. *Immunity* **14**, 523–534 (2001).
53. S. Malstrom, E. Tili, D. Kappes, J. D. Ceci, P. N. Tsichlis, Tumor induction by an Lck-MyrAkt transgene is delayed by mechanisms controlling the size of the thymus. *Proc. Natl. Acad. Sci. U.S.A.* **98**, 14967–14972 (2001).
54. C. Mao, E. G. Tili, M. Dose, M. C. Haks, S. E. Bear, I. Maroulakou, K. Horie, G. A. Gaitanaris, V. Fidanza, T. Ludwig, D. L. Wiest, F. Gounari, P. N. Tsichlis, Unequal contribution of Akt isoforms in the double-negative to double-positive thymocyte transition. *J. Immunol.* **178**, 5443–5453 (2007).
55. F. Gounari, I. Aifantis, K. Khazaie, S. Hoeflinger, N. Harada, M. M. Taketo, H. von Boehmer, Somatic activation of beta-catenin bypasses pre-TCR signaling and TCR selection in thymocyte development. *Nat. Immunol.* **2**, 863–869 (2001).
56. Z. Guo, M. Dose, D. Kovalovsky, R. Chang, J. O'Neil, A. T. Look, H. von Boehmer, K. Khazaie, F. Gounari, β-catenin stabilization stalls the transition from double-positive to single-positive stage and predisposes thymocytes to malignant transformation. *Blood* **109**, 5463–5472 (2007).
57. P. Polakis, Wnt signaling and cancer. *Genes Dev.* **14**, 1837–1851 (2000).
58. J. Roose, G. Huls, M. van Beest, P. Moerer, K. van der Horn, R. Goldschmeding, T. Logtenberg, H. Clevers, Synergy between tumor suppressor APC and the beta-catenin-Tcf4 target Tcf1. *Science* **285**, 1923–1926 (1999).
59. A. Janowska-Wieczorek, M. Majka, J. Kijowski, M. Baj-Krzyworzeka, R. Reca, A. R. Turner, J. Ratajczak, S. G. Emerson, M. A. Kowalska, M. Z. Ratajczak, Platelet-derived microparticles bind to hematopoietic stem/progenitor cells and enhance their engraftment. *Blood* **98**, 3143–3149 (2001).
60. Z. Hao, K. Rajewsky, Homeostasis of peripheral B cells in the absence of B cell influx from the bone marrow. *J. Exp. Med.* **194**, 1151–1164 (2001).
61. I. S. Trowbridge, C. Mazauskas, Immunological properties of murine thymus-dependent lymphocyte surface glycoproteins. *Eur. J. Immunol.* **6**, 557–562 (1976).
62. R. G. Scollay, E. C. Butcher, I. L. Weissman, Thymus cell migration: Quantitative aspects of cellular traffic from the thymus to the periphery in mice. *Eur. J. Immunol.* **10**, 210–218 (1980).
63. Y. Dong, X. Du, J. Ye, M. Han, T. Xu, Y. Zhuang, W. Tao, A cell-intrinsic role for Mst1 in regulating thymocyte egress. *J. Immunol.* **183**, 3865–3872 (2009).

Acknowledgments: We thank J. Woodgett (Lunenfeld-Tanenbaum Research Institute) for providing *Gsk3a*$^{fl/fl}$ and *Gsk3b*$^{fl/fl}$ mice, M. Li (Memorial Sloan Kettering Cancer Center) and Z. Fan (Institute of Biophysics) for providing *Foxo1*^{AAA} mice, C. Liu (Huazhong University of Science and Technology) for providing *Rictor*$^{fl/fl}$ mice, H. Chi (St. Jude Children's Research Hospital) for providing the RV-Akt DN plasmid, and S. R. Schwab (New York University) for providing the $S1P_1$ staining protocol. **Funding:** This study is supported by the National Natural Science Foundation of China (31570882 and 31770950 to W.-H.L., 31770953 to C.X., 31570883 and 31770955 to N.X., 31770952 and 31570911 to G.F., and 81871298 to X.H.), 1000 Young Talents Program of China (N.X.), and the Fundamental Research Funds for the Central Universities of China-Xiamen University (20720150065 to N.X. and G.F. and 20720170064 to C.X.). The funders had no role in study design, data collection and analysis, decision to publish, or preparation of the manuscript. **Author contributions:** W.-H.L., C.L., and L.M. conceptualized and designed the project. C.L. and L.M. performed most of the experiments, interpreted the results, and prepared the manuscript. Yuxuan Wang performed most of retroviral transduction of hematopoietic stem cells (HSCs) and bone marrow reconstitution. X.C. and C.L. performed intrathymic injection and homing experiments under the supervision of G.F. C.L., L.M., P.C., W.-H.L., and C.X. contributed to data interpretation and discussions. W.-H.L., C.X., and C.L. wrote the manuscript with contribution from all authors. W.-H.L. and C.X. supervised the project. **Competing interests:** The authors declare that they have no competing interests. **Data and materials availability:** The *Gsk3a*$^{fl/fl}$ and *Gsk3b*$^{fl/fl}$ mice can be provided by pending scientific review and a completed material transfer agreement. Requests for the *Gsk3a*$^{fl/fl}$ and *Gsk3b*$^{fl/fl}$ mice should be submitted to J. Woodgett (Lunenfeld-Tanenbaum Research Institute). The RNA sequence data are available from the NCBI Sequence Read Archive (BioProject: PRJNA650296). All data needed to evaluate the conclusions in the paper are present in the paper and/or the Supplementary Materials.

Submitted 18 January 2021
Accepted 19 August 2021
Published 8 October 2021
10.1126/sciadv.abg6262

Citation: C. Liu, L. Ma, Y. Wang, J. Zhao, P. Chen, X. Chen, Y. Wang, Y. Hu, Y. Liu, X. Jia, Z. Yang, X. Yin, J. Wu, S. Wu, H. Zheng, X. Ma, X. Sun, Y. He, L. Lin, Y. Fu, K. Liao, X. Zhou, S. Jiang, G. Fu, J. Tang, W. Han, X. L. Chen, W. Fan, Y. Hong, J. Han, X. Huang, B.-A. Li, N. Xiao, C. Xiao, G. Fu, W.-H. Liu, Glycogen synthase kinase 3 drives thymocyte egress by suppressing β-catenin activation of Akt. *Sci. Adv.* **7**, eabg6262 (2021).